EFFECT OF BASALT FIBERS ON THE FLEXURAL BEHAVIOR OF BEAMS REINFORCED WITH BFRP BARS

by

Abdul Rahman M.Musif AlHafiz

A Thesis Presented to the Faculty of the
American University of Sharjah
College of Engineering
in Partial Fulfillment
of the Requirements
for the Degree of

Master of Science in
Civil Engineering

Sharjah, United Arab Emirates

May 2018

© 2018 Abdul Rahman M.Musif AlHafiz. All rights reserved

Approval Signatures

We, the undersigned, approve the Master's Thesis of Abdul Rahman M.Musif AlHafiz.

Thesis Title: Effect of Basalt Fibers on The Flexural Behavior of Beams Reinforced With BFRP Bars

Signature	**Date of Signature** (dd/mm/yyyy)
_____	_____
Dr. Farid Abed Professor, Department of Civil Engineering Thesis Advisor	
_____	_____
Dr. Sami Tabsh Professor, Department of Civil Engineering Thesis Committee Member	
_____	_____
Dr. Mohammad Nazzal Associate Professor, Department of Mechanical Engineering Thesis Committee Member	
_____	_____
Dr. Robert Houghtalen Head, Department of Civil Engineering	
_____	_____
Dr. Ghaleb Husseini Associate Dean for Graduate Affairs and Research College of Engineering	
_____	_____
Dr. Richard Schoephoerster Dean, College of Engineering	
_____	_____
Dr. Mohamed El-Tarhuni Vice Provost for Graduate Studies	

Acknowledgment

Foremost, I would like to thank Allah, the most gracious, the most merciful, for his assistance, and blessings.

I would like to express my sincere gratitude to my advisor, Dr. Farid H. Abed for his support and most appreciated guidance throughout this research. His patience, motivation, enthusiasm, and immense knowledge led to the successful completion of this Master's thesis. Furthermore, his innovative and creative research scope helped in the implementation of the Fiber-Reinforced Polymers behaviour as a new material into the area of reinforced concrete structures. Besides my advisor, I would like to thank my thesis committee members Dr. Sami Tabsh and Dr. Mohammad Nazzal for their fairness, encouragement and insightful comments. Many thanks to the civil engineering department at the American University of Sharjah for their support through the Graduate Teaching Assistantship which helped me to complete my degree and supplied me with vast experience. Special thanks to Mr. Arshi and Mr. Ansari from American University of Sharjah and to Mr. Muttaz from Jamix readymix, who helped me to complete my research works.

Dedication

I must express my very profound gratitude to my parents and brothers for providing me with unfailing support and continuous encouragement throughout my years of study and through the process of researching and writing this thesis. This accomplishment would not have been possible without them. Thank you

Abstract

Over the last few decades, construction materials have gone through many developments aimed at improving their structural and operational properties. The implementation of fiber-reinforced polymer (FRP) bars as a replacement for conventional steel reinforcement in reinforced concrete structures has gained significant acceptance in the construction field. Basalt Fiber-Reinforced Polymer (BFRP) bars are a new type of FRP reinforcement material that was recently introduced to the construction industry. The main shortcoming associated with the use of the BFRP bars in concrete beams is related to the brittle behavior of these beams. This research investigates, experimentally and analytically, the effects of using different types of fibers within the concrete mix on the flexural behavior of BFRP-reinforced concrete beams. The experimental program consisted of material evaluation and flexural testing. A total of 12 beams were prepared and cast using plain, basalt fiber, and synthetic fiber-reinforced concrete with a 40MPa target compressive strength. Flexural testing was conducted on each of the BFRP-FRC beams using a four-point loading test. Results showed a noticeable improvement in the flexural capacities of these beams due to the delay in concrete failure strain (beyond 0.003) at the compression zone, which helped the BFRP bars to attain a higher ultimate strength. Results also indicated that introducing fibers to the concrete increased curvature ductility. Furthermore, the flexural capacity of the section increased by 12% for the basalt fibers RC beams compared to 19% for specimen with synthetic fibers. The opening of cracks and their deep propagation was effectively restrained by the bridging effect of the fibers, which keeps the crack widths lower than the allowable limit of 0.7 mm at the service stage. In addition, the applicability of ACI 440-1R-06 recommendations was assessed using the results of plain concrete specimen and extended to cover fiber-reinforced concrete beams. The experimental results showed good agreement with the analytical ones obtained using ACI equations in terms of flexural capacity, crack spacing, crack widths and mid-span deflection.

Search Terms: ***FRP, FRC, Flexural behavior, BFRP bar, GFRP bar, Fibers, Deflection***

Table of Contents

List of Figures

List of Tables

Chapter 1. Introduction

Developments in construction have resulted in introducing new materials as reinforcing bars in structural members. Each material has its own shortcomings in delivering the predicted performance. The inherently corrosive nature of conventional steel reinforcement is one of the most commonly occurring problems that increases the need for alternative solutions. Fiber-reinforced polymer (FRP) composites have been used in structural engineering for almost 50 years for both, restoration of existing structures and new construction [1]. The implementation of fiber-reinforced polymer (FRP) bars as a replacement for conventional steel reinforcement in reinforced concrete structures has gained significant acceptance in the construction field. FRP bars are a non-corrosive and nonmagnetic material, which makes them perfectly appropriate for reinforcing concrete structures in harsh environments [2]. There are many types of FRP materials used as reinforcement to resist both shear and flexural stresses in concrete structures. Glass fiber-reinforced polymer (GFRP), carbon fiber-reinforced polymer (CFRP) and aramid fiber-reinforced polymer (AFRP) are the most common types of FRP composite reinforcement. In the last few years, manufacturers' and researchers' attention has been attracted to the promising features of basalt FRP (BFRP) as a new reliable reinforcing material [3] [4]. In terms of flexure and serviceability, BFRP bars have the same characterization as other FRP composites. In addition to their corrosion resistance, BFRP bars have a high tensile strength-to-weight ratio, which leads to a sufficiently desirable strength together with an easy handling and erection process. Unlike conventional steel reinforcement, FRP bars behave elastically until failure, which translated into a lack of ductility[5]. In addition, FRP bars as reinforcement have a low modulus of elasticity compared to steel [2], [4], [6]–[15]. For instance, glass and aramid FRP composites have elastic moduli ranging from 35 to 50 GPa, which is approximately 21% of the elastic modulus of steel, commnly around 200 GPa. Moreover, FRP bars have a high tensile strength that can exceed 1000 MPa [15].

The most prominent concern in flexural members reinforced with BFRP is their brittle behavior. BFRP bars do not yield; therefore, they have a linear elastic behavior until failure [2]–[4], [6]–[9], [11]–[17]. This could result in catastrophic failure without any precautions, which is not desirable by designers.

The American standards and design code for fiber-reinforced polymer as longitudinal reinforcement, ACI 440-1R-06 [18], allows two modes of flexural failure to be used in the design of FRP-reinforced concrete members [17]. The first failure mode is controlled by FRP rupture. This mode of failure is similar to the tension-controlled failure which is adopted by the ACI-318 code for steel reinforcement. Since FRP bars have no yielding point, the precautions before failure are limited and the member experiences a sudden and catastrophic failure. The second failure mode is controlled by concrete crushing (compression-controlled). According to ACI 440-1R-06, in order to design a section that can fail by FRP rupture, the FRP reinforcement ratio should be less than the FRP balanced reinforcement ratio ($\rho_f < \rho_{fb}$). In contrast, concrete crushing failure can be accomplished by using an FRP reinforcement ratio that is greater than the FRP balanced reinforcement ratio ($\rho_f > \rho_{fb}$) [17].

Researchers have performed many investigations that aim to develop a suitable solution to improve the ductility of the concrete members reinforced with FRP. Since FRP bars have no yielding strain and since it is preferable that concrete crushing occur before the FRP bars rupture, the challenge is to improve the compressive strain properties of concrete in order to postpone concrete crushing and allow FRP bars to contribute more to the load carrying capacity [6], [8], [13], [15], [19]. Incorporating randomly distributed micro fibers into the concrete mix is one solution to overcome the problems of ductility and deformability of FRP-Reinforced concrete members.

Several types of fibers such as steel fibers, synthetic polypropylene fibers, and the newly developed Basalt fibers, have been used in the FRP-FRC system [15]. Basalt chopped fibers are available in lengths ranging from 12 to 100 mm and diameters ranging from 10 to 20 μm. Basalt fiber exists in filament and bundled form [20], [21].Once microcracks develop in a structural concrete member, basalt fibers will sustain the stresses and restrict cracks propagation as load is applied by the mean of bridging effect. Unlike plain concrete which is weak in tension, it will not be able to sustain the stresses and hence, the cracks continue to propagate and elongate [21].

1.1. Problem Statement

Although concrete is a brittle material, studies have shown that the compression-controlled failure mode exhibits more plasticity than the tension-controlled one. Since compressive concrete properties can be enhanced, compression-

controlled failure is recommended as it provides more precaution before failure. Studies had proven that the effect of the fibers on concrete properties depends on the length and dosage of the fibers in the concrete mix [20]–[23]. In addition, studies have shown that the optimum dosage of Basalt fibers to allow the best mechanical properties to be achieved ranges between 0.3-0.8% of the total volume of the concrete mix [21], [23], [24]. In this study, chopped Basalt fibers of 12 and 24 mm length and a volume fraction of 0.75% of the total volume of the mix are used. Generally, adding fibers to the concrete mix can improve its mechanical properties including flexure, deformation, toughness, ductility and load carrying capacity after cracking [23]. Bridging the micro and macro-cracks in the structural member is the main function of the short and long fibers. Consequently the post-cracking behavior of FRP-reinforced concrete members is improved [21].

1.2. Research Significance

As technology in the construction field advances, the need for developing new construction materials that can overcome the weaknesses of conventionally-used materials increases. Both the structural and economical sides should be considered when introducing a new material or technique**.** FRP composites are one of the recently used materials as a replacement of conventional steel in reinforcing concrete structures. Lately, Basalt fiber-reinforced polymer (BFRP) bars show promising features that may overcome the shortcomings of steel and other FRP reinforcing materials. The flexural performance of BFRP bars showed a significant acceptance in previous studies. Since the BFRP-reinforced concrete [BFRP-RC] beams are designed to fail by concrete crushing (compression control) as preferred by the ACI 440-1R-06 code[18], the concrete's ultimate strain should be increased in order to add some ductility to the FRP beams and utilize as much of the BFRP high tensile strength as possible. This phenomenon can be accomplished by the addition of discrete fibers to the concrete mix.

In this research study, the effect of using different types of micro fibers, reinforcement ratios and reinforcement bars on the flexural behavior of concrete beams reinforced longitudinally with BFRP bars is evaluated. The study includes experimental work in addition to some analytical work for comparison purposes. Consequently, the significance of this research lies mainly in utilizing both, the high tensile strength of the BFRP bars as longitudinal reinforcement and the ductility provided by introducing fibers to the concrete mix. This will result in an optimum beam section that has the

highest flexural capacity and controlled cracking behavior. Documenting the behavior of BFRP-FRC cast with different types of fibers is expected to reduce the uncertainty related to using FRP as longitudinal reinforcement in flexural members. Therefore, this could encourage building-code committees such as the ACI 440-1R-06 to consider this type of systems to be applicable for flexural applications.

1.3. Research Objectives

The main objective of this study is to investigate the effect of the addition of basalt fibers to the concrete mix on the flexural behavior of concrete beams reinforced longitudinally with BFRP bars. Since the ACI 440-1R-06 code recommends compression control as a failure mode for the FRP reinforced beams, there is a significant need to improve the concrete's ultimate compressive strain in order to utilize the high tensile strength of longitudinal BFRP bars and improve the load-carrying capacity. Generally, plain concrete beams reinforced with FRP bars are designed to fail at a concrete strain of 0.003. This consequently results in a reduced utilization of the tensile strength of FRP bars. Therefore, adding fibers to the concrete is expected to allow the compressive strain to exceed 0.003 and give the concrete a tendency towards improved flexural behavior in terms of cracking response, deflection and ductility. The objectives of this research can be summarized as follows:

1) Enhance concrete properties by introducing fibers (basalt and synthetic) into the concrete mix to achieve a concrete mix with high strength, high ductility, and improved cracking control, which are the main features of FRC.
2) Study the flexural behavior of the FRC beams reinforced with BFRP bars considering different reinforcement ratios by conducting a four-point bending test and comparing the results to those of beams reinforced with GFRP and steel. From this comparison, capture any enhancement in the ultimate compression strain at the top concrete fibers at mid-span. Additionally, monitor the cracking behavior and crack widths at different loading stages.
3) Investigate the effect of using different numbers of BFRP longitudinal bars with the same flexural stiffness on the overall flexural behavior of reinforced beams.
4) Implement an analytical program to assess the applicability of the ACI 440-1R-06 recommendations in calculating the flexural capacity, crack widths, crack spacing and deflection of beams cast with either plain or FRC mixes and reinforced longitudinally with BFRP bars.

1.4. Thesis Structure

The thesis starts with the introduction chapter which introduces the BFRP material and explains its advantages when used as longitudinal reinforcing bars in flexural members. The chapter also states the problem being studied and its significance. The second chapter gives the background necessary to understand the properties of different materials used in the research such as: BFRP, GFRP, and FRC. Chapter 2 also introduces and summarizes the research outcomes of other studies conducted by many researchers on the flexural behavior of concrete members reinforced longitudinally with materials exhibiting high tensile strength (similar to BFRP) such as GFRP and CFRP. Chapter 3 defines the implemented experimental program in detail. It shows the test matrix, test setup and instrumentation for the flexure test. The current design guidelines and equations for the FRP-RC beams are summarized in chapter 4 for the determination of flexural capacity, cracking behavior and mid-span deflection. The results of the experimental program are summarized in Chapter 5 and discussed in Chapter 6 to capture the main effect of using a variety of fiber types such as basalt or synthetic fibers, different reinforcement ratios, and different reinforcement materials (BFRP, GFRP and steel) on the overall flexural behavior. Chapter 7 assesses the design guidelines based on the experimental results including flexural capacity, crack behavior and mid-span deflection. The thesis ends with Chapter 8 which states the main conclusions and provides several recommendations for structural designers.

Chapter 2. Literature Review

In this chapter, a review of the literature is done, focusing on related studies and experimental programs.

2.1. Overview of Fiber-Reinforced Polymer (FRP) Properties

Fiber Reinforced Polymer (FRP) material is a kind of composite material that is manufactured by combining small-diameter fibers with a polymeric matrix at a microscopic level to produce a synergistic material [1]. It has been used often in the construction industry in recent years. This high demand is due to the material's light weight, high tensile strength, nonconductive behavior, nonmagnetic nature, high corrosion resistance, and simple implementation procedure. These features make the material a preferable solution for both, strengthening reinforced concrete structures and reinforcing new structural elements.

2.1.1. Production of FRP. FRP composites have been implemented in an extensive range of applications in different fields including bridges, airport facilities, retaining walls, and especially, structures exposed to aggressive environments [25]. There are many types of manufacturing processes that are used to produce the FRP composites. The most commonly used one is the pultrusion process. Pultrusion is a continuous manufacturing process which can produce one to five feet per minute of prismatic thin-walled members [25]. FRP composites can be produced into three different materials; solid continuous bars and plates, fully structural profiles, and short discrete fibers. The bars shown in Figure 1 are mainly used as internal reinforcement or are externally bonded to structural concrete for strengthening purposes. On the other hand, the structural profiles shown in Figure 2 are implemented in the bridge construction field, either as piers or as bridge deck slabs [1], [25]. The short discrete fibers shown in Figure 3 are another type of FRP material that is recently used in concrete mixes in order to improve the compressive strain of concrete, thereby increasing its flexural capacity.

In the following sections, some of the most important FRP properties that are relevant to their application in the construction field are discussed briefly.

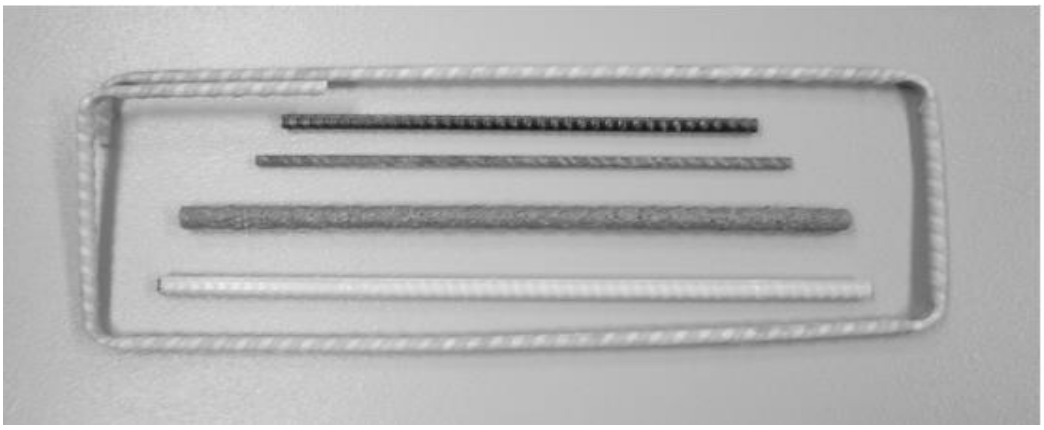

Figure 1: FRP bars [1]

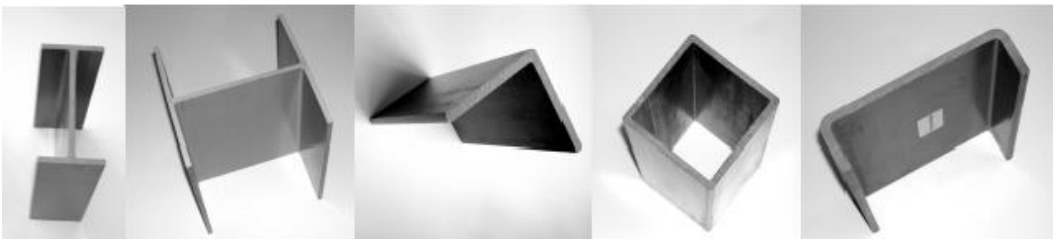

Figure 2: FRP composite profiles [1]

Figure 3: Basalt Fibers[26]

2.1.2. Compressive strength. The difficulty in examining the compressive strength of FRP materials is due to their brittleness and tendency to buckle, and the lack of information available on this matter. It has been stated that the compressive strength and modulus of elasticity of Kevlar fibers are significantly lower in compression than they are in tension [27]. With the limited studies and information on the compressive performance of FRP, publishing data in this subject remains a challenge for structural

engineers and researchers.

2.1.3. Tensile strength and modulus of elasticity. FRP composites vary in tensile strength based on many parameters including the type and content of the fiber and the type of the resin used in manufacturing process. While GFRP offers a tensile strength that is nearly equal to or slightly greater than mild steel yield strength, CFRP composites exhibit a tensile strength that varies between two to five times the yield strength of mild steel. Both FRP composites have a tensile stiffness lower than that of steel [1]. Unlike steel bars, studies have proven that FRP bars have a linear elastic behavior until failure, which means that there is no strain hardening stage.

A study carried out by Uomoto and Nishimura 1994 [27] aimed to investigate the variations of tensile strength and elastic modulus with the type and content of fibers used in manufacturing the FRP. For that purpose, 100 specimens were prepared using different parameters. The study concluded that the fracture strain of FRP was much lower than that of steel, which is why structures reinforced with FRP should be designed based on the serviceability limit state rather than the strength limit state. In addition, the elastic modulus of FRP material was found to be half that of steel. However, the tensile strength of FRP materials was much higher than that of conventional steel. Also, the study showed that as the fiber content (V_f) in the FRP increased, the tensile strength and elastic modulus increased as well.

A comparison of the mechanical properties of the different types of FRP, as summarized in Table 1, shows that carbon composite exhibits a stiffness of two to five times that of the glass composites. Additionally, FRP composites have almost one-fifth the weight of steel. The tensile properties of FRP strengthening systems can be obtained either directly from the FRP manufacturer or using the test method mentioned and described in ASTM D7565 [27]. The ACI 440.6-08 states that GFRP and CFRP reinforcing bars have a tensile elastic modulus of no less than 39.3 GPa (5700 ksi) and 124 GPA (18,000 ksi), respectively [17]. Figure 4 shows stress-strain curves for different types of FRP composites.

Table 1:Properties of FRP composites [1]

Parameter	V_f	fiber type	AFRP	GFRP	CFRP
Strength (K_{gf}/mm^2)	45	Mean value	135	140	124
		SD	9.49	5.83	11.8
		COV	0.0703	0.0416	0.0952
	55	Mean value	169	169	134
		SD	14.8	8.53	11.2
		COV	0.0876	0.0505	0.0836
	66	Mean value	204	177	148
		SD	5.73	12.2	27
		COV	0.0281	0.0689	0.1824
Elastic modulus (K_{gf}/mm^2)	45	Mean value	3748	4274	11202
		SD	216.1	52.2	259.5
		COV	0.0576	0.0122	0.0232
	55	Mean value	4570	5211	13530
		SD	194.5	47.6	236.3
		COV	0.0426	0.0091	0.0175
	66	Mean value	5460	6024	15714
		SD	241.2	101.2	379.4
		COV	0.0442	0.0168	0.0241

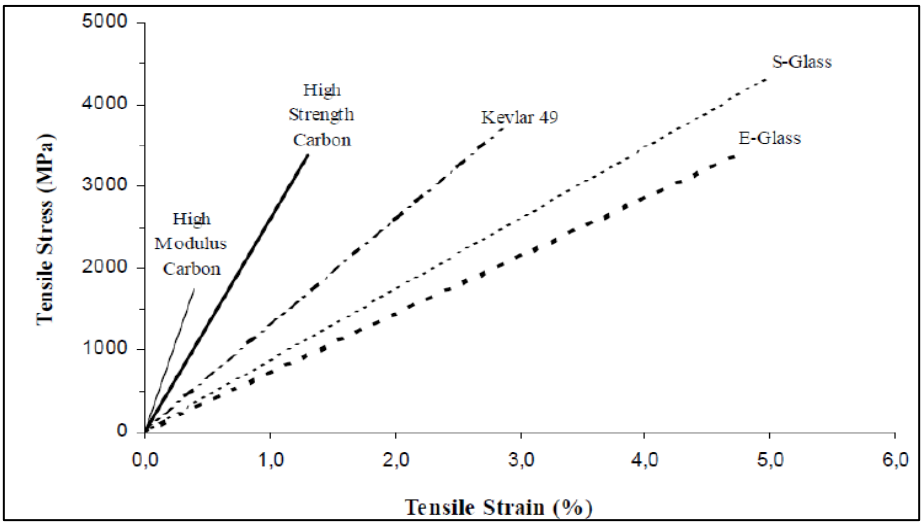

Figure 4: Stress-Strain curves of different FRP composites [1]

2.1.4. Deflections and cracking. Deflections and crack widths in FRP reinforced concrete structures and particularly in GFRP reinforced structures are usually larger than in steel-reinforced concrete beams due to the low elastic modulus of FRP. Specifications on deflection or crack width often control designs and usually, the solution for such deflections is the use of over-reinforced sections. At lower loads, the cracking response of the FRP structures is close to that of conventional steel structures. As the loads increase and get closer to the ultimate, the crack widths and deflections in the FRP structures become larger than steel structures [1], [6], [27], [28]. American Concrete Institute (ACI-440) code equations for deflections can also be used for FRP reinforcement [17].

2.1.5. Bond strength and development length of reinforcement. The bond characteristics of FRP reinforcing bars are one of the bars' most important features and they vary from one product to another. Compared to the bond strength of steel reinforcement, some FRP materials have higher bond strengths, while others exhibit lower bond strengths[29]. The bond strength of FRP reinforced concrete members is a function of the bar surface and concrete cover [30][10]. For instance, bars with helical wraps on the surface have additional bond strength through the mechanical interlock, which makes the bars more dependent on the concrete cover. Another factor that affects the bond strength of FRP reinforced concrete members is the development length [29]. According to ACI 440, local bond-slip relations have been conducted on glass FRP reinforcement and based on the test results, the minimum development length of glass FRP bars required to avoid failure by pull-out is in the range of 26-37 times the bar diameter [17].

A study was conducted by El Refai et al in 2015 [31] to investigate the bond behavior of Basalt fiber-reinforced polymer (BFRP) bars to concrete. 63 concrete cylinders were reinforced with BFRP, and 12 concrete cylinders were reinforced with Glass FRP (GFRP) for comparison purposes. The beams were tested in direct pull-out tests. Based on the test results, both the BFRP and the GFRP bond-slip curves showed the same trends; however, the BFRP cylinders showed an average bond strength equivalent to 75% that of the GFRP. The failure of the BFRP bars occurred along the interfacial surface between the outer layer and the core layer of the bar [31].

2.2. Glass-Fiber Reinforced Polymer Rebars (GFRP)

Glass FRP has been widely used as longitudinal reinforcement in structural members. Many studies have investigated the GFRP's performance in flexure and shear. Glass is a shapeless inorganic compound that mainly consists of Silica dioxide (SiO2). There are many classes of glass fiber available in the market. E-glass (electrical glass) is a borosilicate glass known for its high electrical resistivity and used to produce the most popular FRP products. Other classes of glass fiber include A-glass (window glass), C-glass and S-glass, which have a high strength and are used to manufacture high-performance fibers for aerospace applications. Table 2 shows the mechanical properties of different classes of glass fibers [1].

Table 2: GFRP mechanical properties [1]

Grade of Glass Fiber	Density [g/cm³ (lb/in³)]	Tensile Modulus [GPa (Msi)]	Tensile Strength [MPa (ksi)]	Max. Elongation (%)
E	2.57 (0.093)	72.5 (10.5)	3400 (493)	2.5
A	2.46 (0.089)	73 (10.6)	2760 (400)	2.5
C	2.46 (0.089)	74 (10.7)	2350 (340)	2.5
S	2.47 (0.089)	88 (12.8)	4600 (667)	3.0

According to the American standard (ACI-440), GFRP bars are produced with the following property ranges: tensile strength (483 to 1600 MPa), elastic modulus (35 to 51 GPa), and rupture strain (1.2 to 3.1 %). Table 3 shows the mechanical properties of GFRP from the manufacturer compared to those of conventional steel reinforcement [17].

Table 3: Comparison between steel and GFRP properties [1]

Mechanical properties	**Bar type**	
	Steel	**GFRP**
Nominal yield stress, Mpa (Ksi)	276 to 517 (40 to 75)	N/A
Tensile strength, MPa (Ksi)	483 to 690 (70 to 100)	483 to 1600 (70 to 230)
Elastic modulus, 10^3 GPa (Ksi)	29 (200)	5.1 to 7.4 (35 to 51)
Yield strain, %	0.14 to 0.25	N/A
Rupture strain, %	6 to 12	1.2 to 3.1

All mechanical properties of FRP bars should be obtained from the manufacturer due to the complexity of the tests needed for strength determination. This complexity is due to the premature failure that occurs as a result of the stress concentrations in and around anchorage points on the test specimen [17]. In addition to its multiple advantages of resisting corrosion and high strength to weight ratio, GFRP have a low cost compared to steel and other FRP products [32].

Habeeb and Ashour [7] conducted a study in 2008 aimed to investigate the flexural behavior of continuous beams reinforced with GFRP. Reinforcement ratio was the main parameter that controlled the experimental program. A number of 2 simply supported and 3 continuous GFRP-reinforced concrete beams were cast together with one continuous steel-reinforced concrete beam for comparison purposes. Some beams were over-reinforced with GFRP and some were under-reinforced either in the bottom or top reinforcement. The results showed that the first mid-span crack in the over-reinforced GFRP beams occurred at a slightly higher load than in the under-reinforced GFRP beams. It could be also noticed that, in the over-reinforced GFRP beams, cracks initiated at the negative moment region (over the middle support). However, in the under-reinforced GFRP beams, cracks initiated at the positive moment region (at the mid-span). The beams exhibited three different failure modes. The first failure mode was failure by FRP rupture, which was experienced by GFRP bottom under-reinforced beams. The second was failure by concrete crushing, which appeared in the GFRP bottom over-reinforced beams. The third mode of failure was by concrete crushing combined with shear failure, which was experienced by GFRP beams with over-reinforcement at the top and bottom. The reason behind the third mode was that, when the beam was over-reinforced at the top and bottom, the compression resistance became very high which allowed shear force to control part of the beam failure. It was also concluded that the GFRP over-reinforced simply supported beams failed at 50% of the total failure load of GFRP over-reinforced continuous beams. A similar trend was noticed for the under-reinforced simply supported beams which failed at 40% of the total failure load of continuous beams.

Since the ACI 440-1R recommended that FRP reinforced concrete beams be designed with over-reinforcement, the properties of concrete became the core of controlling the flexural behavior[33]. Implementing the advantages of high and ultra-high strength concrete is one of the methods that were predicted to improve concrete

compressive properties and increase the failure strain. An experimental study carried out by Goldston, et al. in 2017 [34] focused on the influence of using high strength concrete (HSC) and ultra-high strength concrete (UHSC) on the flexural behavior of 9 GFRP beams. In addition, three steel reinforced concrete beams were cast for comparison purposes. Three main variables controlled the testing program: concrete compressive strength (80 and 120 MPa), the reinforcement ratio ρf considering both over-reinforced and under-reinforced cases, and the size of the GFRP bar. The study concluded that the GFRP beams retain the trend of elastic linear behavior until failure even with the use of HSC and UHSC. It was also noticed that increasing concrete strength from HSC (95 MPa) to UHSC (117 MPa) increased the load carrying capacity of the over-reinforced beams by 27% and 13% for reinforcement ratios ρf=1 % and ρf=2%, respectively. It also increased the post cracking stiffness for beams of the same reinforcement ratio. Moreover, the over-reinforced beams exhibited a more ductile behavior compared to the under-reinforced beams. The test results also showed that by increasing the reinforcement ratio using UHSC, the ductility increased. For the HSC and UHSC GFRP-RC beams with reinforcement ratios of ρf = 1.0% and ρf = 2.0%, the total energy absorption capacity increased by 4% and 5%, respectively, for an increase in concrete strength from 95 MPa (HSC) to 117 MPa (UHSC).

2.3. Basalt Fiber-Reinforced Polymers Rebars (BFRP)

Recently, efforts in developing fiber-reinforced polymer (FRP) technologies have concentrated on using a new type of fiber, Basalt fiber-reinforced polymer (BFRP). Basalt FRP is anticipated to give advantages comparable to or better than those of other FRP types, while being significantly more cost-effective. BFRP reinforcing bars have advantages that exceed those of other FRP bars such as Carbon FRP (CFRP), Glass FRP (GFRP), and Aramid FRP (AFRP). For instance, BFRP is more chemically stable than E-glass FRP and has a higher tensile strength and elastic modulus. In addition, it has a varied range of working temperatures and a much lower cost than CFRP [4].

Limited studies investigating the structural behavior of BFRP are available. In 2016, Elgabbas, Ahmed and Benmokrane [4] conducted a study to examine the flexural behavior of RC beams reinforced with Basalt FRP bars under static loads. For that purpose, six beams reinforced with 8,12 and 16 mm BFRP bars with ripped surfaces were tested and compared with two reference steel RC beams with 10 and 15mm steel

bars. All the BFRP beams were designed to fail by concrete crushing, while the steel beams were under-reinforced to fail by steel bar yielding. Both ACI and Canadian Standards Association (CSA) were used to predict theoretical results that were then compared with the experimental results. The test results showed that as reinforcement ratio increased (become more over-reinforced), the ultimate capacity increased in such a way that a 50% increase in the BFRP reinforcement ratio increased RC beam capacity by 28%. Since BFRP bars have higher tensile properties and stiffness than GFRP bars, BFRP bars have proven their ability to carrying more loads before concrete crushing. It was also noted that the ultimate capacity of BFRP beams is higher than that of steel beams. The test also included bond coefficient (Kb) determination based on ACI and CSA codes. The results showed an average Kb value of 0.83 for the ripped BFRP bars which is less than the value provided by CSA standards, 1.

Another study conducted by Tomlinson and Fam in 2014 [12] focused on the flexural and shear behavior of BFRP RC beams. Nine beams with (150 × 300 × 3, 100-mm) dimensions were cast and tested in four-point bending to investigate the influence of BFRP flexural reinforcement ratios varying from 0.28 to 1.60 the balanced ratio on the structural performance. The beams were reinforced by either BFRP bars or steel stirrups, and some had no shear reinforcement at all. The test results showed that the flexural reinforcement ratio proportionally affects the ultimate and service loads. However, the service loads were not influenced by stirrup type. The failure mode differed from one beam to another based on the shear reinforcement. Beams with BFRP stirrups failed by stirrups rupture, with a capacity that reached up to 90-96% of the ultimate flexural strength. Beams without stirrups failed in shear with a capacity of 55-58% of the ultimate flexural strength. On the other hand, beams with steel stirrups failed in flexure.

2.4. Fiber-Reinforced Concrete (FRC)

When the concrete matrix is mixed with discrete short fibers, the resulting material is fiber reinforced concrete (FRC). This mixture can be done using a binding agent, which is usually epoxy and polyester resins. The fibers efficiently improve the compressive properties of the concrete. The compressive strength of the FRC can exceed (120 MPa) if the mixing and curing processes are done properly [35].

In 2016, Branston et al. [26] conducted a study to evaluate the role of basalt fiber-

reinforced concrete in enhancing the mechanical behavior of concrete. Concrete specimens were cast using two types of Basalt fibers with three different quantities and then tested in flexure. The basalt fibers used were bundled dispersion and minibars. Steel fibers were used for comparison purposes. The test results showed that the addition of fibers to concrete does not increase the compressive strength of the specimens. The compressive strength even decreased for the specimens containing minibar-fiber basalt and those containing steel fibers due to the low workability which resulted in less consolidation of the fibers within the matrix. However, the addition of fibers to the concrete significantly influenced the flexural behavior in terms of cracking load and deflection. The results showed that with the addition of bundled basalt fibers, the first cracking strength increased with increases in fiber dosage and length. For instance, a 12 kg/m3 dosage of 50 mm bundled fibers resulted in a first-cracking strength that was comparable to a dosage of 40 kg/m3 of steel fibers (see Figure 5). In addition, the bundled fibers had no effect on the post-cracking strength of the specimen. On the other hand, the minibar basalt fibers had a potential effect on both the first-crack and post-crack strength. As the minibar basalt dosage increased, the first-cracking strength increased such that a dosage of 20 kg/m3 of minibar basalt fibers resulted in a comparable increase in first-crack strength to that of steel fibers with a dosage of 40 kg/m3. The difference between bundled and minibar basalt fibers is that minibar fibers have a higher ductility than bundled fibers; therefore, the minibar-fiber containing specimens failed by fiber pull-out while the bundled-fiber containing specimens failed by fiber rupture. Hence, the minibar-fiber specimens had an improved post-cracking strength. Figure 5 shows the load versus midspan deflection for both of the fibers type.

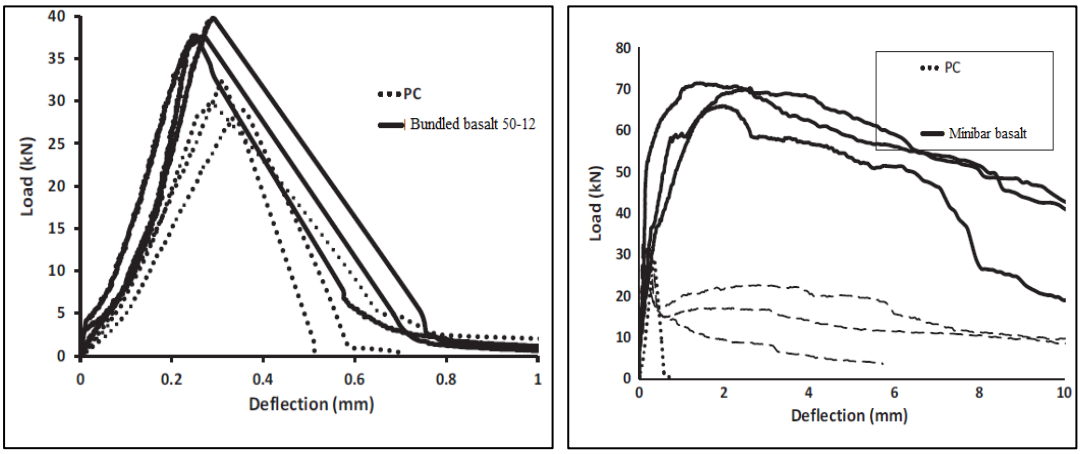

Figure 5:Load-Deflection (Bundled fibers Vs Minibar fibers)[26]

Another study conducted by Reis, J [36] aimed to compare between the mechanical properties of fiber reinforced epoxy polymer concrete (FRC) and conventional concrete. The data obtained from compressive tests showed that fiber reinforcement has a good influence on the compressive strength of epoxy polymer concrete. While the carbon fiber reinforced concrete (CFRC) showed a significant improvement of 16% in the compressive strength of the concrete, the glass fiber reinforced concrete (GFRC) showed only 8.7% of improvement [36]. The behavior changed when elastic modulus was analyzed. Neither the carbon fiber reinforced polymer composite (CFRPC) nor the glass fiber reinforced polymer composite (GFRPC) indicated any improvement in elastic modulus. On the other hand, a slight decrease was observed in CFRPC compared to plain and glass reinforced concrete. The value of Poisson's ratio for all concrete samples did not indicate any noticeable trend. When compared to market concrete, plain epoxy concrete exhibited a higher compressive strength, with increase values ranging between 17 to 34%. In the same way, the compressive strength values of GFRPC were higher in the range of 28 to 45%. Carbon fiber reinforced epoxy polymer concretes exhibited much higher values of compressive strength than conventional concrete by a range of 36 to 55 % [36]. Table 4 below shows the test results in terms of compressive strength, compressive modulus and Poisson's ratio.

Table 4:comparison between plain concrete and glass and carbon fiber reinforced concrete [25]

Test Series	Compressive Properties (Average)		
	Strength (MPa)	Elastic. Modulus (GPa)	Poisson's Ratio
Plain	59.681	11.281	0.259
CFRPC	69.215	10.882	0.247
GFRPC	64.873	11.551	0.257

Another study, conducted by Campione in 2012 [37], aimed to investigate the influence of steel fibers on the flexural behavior of reinforced concrete deep beams. Four beams were cast for this study: two made with plain concrete and steel longitudinal reinforcing bars and two made with hooked steel fibers with steel reinforcement longitudinally. A four-point bending test was conducted on each beam to evaluate the flexural performance in the form of cracking response, load-deflection behavior and the ductility of the beam. The study concluded that adding steel fibers to the concrete mix

increases the strength and ductility of the reinforced concrete beams. The test showed that the beams exhibited similar linear uncracked behavior until the first diagonal cracking, followed by nonlinear cracked behavior up to the peak load. Once the peak load was reached, the RC beams experienced a sudden failure, while the SFRC sustained higher loads with more ductile behavior.

2.5 Fiber-Reinforced Polymer with Fiber-Reinforced Concrete (FRP-FRC)

Many studies have proved that the strength of the reinforced concrete (RC) beams can be increased by using concrete with higher strength, increasing the amount of reinforcement, or changing the dimensions of the beam. All these variables have the ability to improve reinforced concrete strength. However, improving the ductility of the section is much more difficult and may not be achieved by these conventional parameters. Using FRP reinforcement together with steel reinforcement in one hybrid system is one of the recently adopted techniques to improve the flexural behavior of concrete structures [38]. The use of fibers in the RC beams is the simplest way to achieve the needed ductility together with higher strength. When fibers are used in the concrete mix with FRP reinforcement, a complete system is developed called "FRP-FRC" which refers to Fiber-reinforced concrete reinforced with fiber-reinforced polymers. This system has gained a wide acceptance as an option to improve the ductility of the FRP reinforced concrete members. Limited studies are available studying the effect of adding fibers to the FRP reinforced concrete beams. These studies showed that by introducing fibers to the FRP reinforced concrete beams, the flexural behavior in terms of ductility, cracking response and deflection can be enhanced [8], [13].

Wang and Belarbi conducted a study in 2010 [13] aimed to evaluate the effect on flexural behavior of combining fiber reinforced concrete (FRC) with continuous fiber-reinforced polymer (FRP) in a single system.. For that purpose, Wang and Belarabi cast a number of 12 beams (178 mm x 229 mm x 2032 mm) separated into six groups. Each group includes two similar beams, one loaded monotonically and the other subjected to repeated loading/unloading. Three parameters mainly controlled the testing procedure namely the FRP rebar size (#4 Vs #8), the FRP reinforcement type (CFRP Vs GFRP), and the existence of randomly distributed polypropylene fiber within the concrete mix (FRC Vs plain concrete). Diameters of the bars used in this test were 25mm and 13mm GFRP and 13mm CFRP. The surface of the GFRP bars was sand

coated helical fiber, while the CFRP surface was made of epoxy modified vinyl ester. Concrete crushing was the predesigned failure mode for all the beams, which was achieved by making the fiber reinforcement ratio greater than the balanced ratio. Concrete strength was designed to achieve 30MPa for FRC and 40MPa for plain concrete at the testing date. All beams were tested using four-point flexural testing. Stirrups of U-shaped No.3 steel were used as shear reinforcement to avoid shear failure, while no stirrups were used in the pure bending region. Each testing parameter was studied using two beams. On one beam, the load was applied monotonically up to failure. On the other beam, a repeated loading/unloading cycle was applied at 40% and 80% of the beam's capacity, to investigate the residual deflection, the residual crack width, and the energy absorption capacity. The study showed that, by adding fibers, the tensile strength of concrete increased by the mean of fibers bridging. This made the beam with FRC able to carry more stresses with less crack spacing at 0.4Mu. At 0.8Mu, fibers started to pull out and fiber-bridging stopped, and thus the crack spacing of the FRC became the same as that of plain concrete. Additionally, the addition of fibers to the concrete reduced the crack width as compared to plain concrete, especially at the service load (0.4Mu). It was also noted that the deflections and moment capacities were higher in the FRC beams than in the plain concrete beams. Specifically, the deflection of the CFRP beams was more than the deflection of the GFRP due to the higher modulus of elasticity of GFRP. The experimental results showed that the concrete strain of the FRC beams was higher than 0.003, which proved the advantage of using fibers in improving the compressive properties of concrete. The study also concluded that crack width, crack distribution, deflection, and flexural stiffness were not affected by the loading/unloading cycles due to the linear elastic behavior of the FRP bars.

Another study conducted by Issa et al. [8] aimed to improve the ductility of concrete beams reinforced with FRP bars. As recommended by the ACI 440, the FRP beams should be over-reinforced to fail by concrete crushing instead of by rupture of the FRP bars [17]. That means a lower ductility will be achieved in the design. Thus, randomly distributed short fibers were added to the concrete mix to investigate their effect on the flexural behavior and ductility of a structural member. A number of seven concrete beams with the same dimensions (150 x 150 x1850 mm) reinforced with glass fiber-reinforced polymer (GFRP) were used as specimens for the experimental program. The study monitored the effect of the concrete grade and the type of the

internal fibers as the controlling parameters for the test. The beams were classified into four groups based on the type of internal fibers ; no fibers (O), polypropylene fibers (P), glass fibers (G) and steel fibers (S) and into two groups based on the concrete grade (normal (N) [25 MPa] and high strength concrete (H) [65 MPa]). The amount of fibers used in all of the beams was 0.5% of each beam's concrete volume. The tested beams showed that adding fibers to the concrete mix improves the ductility of the beams. This effect was especially prominent with the steel fibers, which increased the ductility by 277.8%. The test results also showed that the ultimate load of the beams was increased considerably by adding fibers compared to the plain concrete. It was also noted that, the mid-span vertical deflection in the FRC beams reached higher values than in the plain concrete beams. For instance, the mid-span deflection of the beam that had steel fibers with normal concrete reached 45.97 mm while, in the plain normal concrete beam, it reached 27.49 mm. Moreover, the concrete strain increased by using fibers. For example, the concrete strain in the NP beam (normal concrete beam containing polypropylene fibers) increased by 33% compared with the normal plain concrete beam.

There are many parameters that can significantly affect the flexural behavior of the FRP/FRC beams. The fibers that are introduced into the concrete mix can influence the strength of the beams through different factors including fiber shape, volume, and type. Based on the fiber type, the shape of the fiber particles can differ. For example, steel fibers can be found in two different shapes, crimped and hooked. The volume fraction of fibers defines the content of fibers as a percentage of the total concrete volume.

Alsayed and Alhozaimy [6] conducted a study on 18 fiber-reinforced concrete beams reinforced with GFRP bars. The study aimed to investigate the effect of adding steel fibers (SF) of different shapes and volume fractions to the concrete mix on the flexural behavior and ductility of the GFRP/FRC beams. All the beams had the same length of 2900 mm. A four-point test was prepared over a clear span of 2700 mm. During the test, many performance characteristics were monitored using a data acquisition system. The applied load was monitored using a load cell, mid-span deflection and support movements were monitored using LVDT, and the strains of the FRP and steel bars were monitored using strain gages. The test results of the cast small beams and cylinders show that, by adding SF to the concrete, the compressive strain in

concrete increased. On the other hand, the four-point test results for the GFRP-reinforced beams showed that the beams containing crimped SF failed by GFRP bar rupture, while the beams containing hooked SF failed by concrete crushing. It was also noted that the deflection of the beam increased by adding SF to the concrete, which reflects the influence of SF in increasing ductility. The study also concluded that hooked SF increased the ductility of the beams more than crimped SF. The addition of 1% hooked SF increased the ultimate load by 16%, increased flexural rigidity by 100%, and reduced the central deflection at the ultimate by 116%.

In addition to the fibers' effect, the FRP reinforcement type also affects the flexural behavior of the FRP/FRC system. A study on this topic was conducted by Yang et al. [15] and aimed to investigate the influence of changing FRP and fiber types on the flexural behavior of FRP/FRC beams. Two types of reinforcement, GFRP and CFRP, were used in this study. Two types of discrete fibers, steel fibers and polypropylene synthetic fibers, were used. The test results showed that the first cracking load of the FRC beams was higher than that of the beams without fibers. This indicates that the tensile strength of the beams increased by the addition of the fibers. The ultimate load of the GFRP/FRC beam with synthetic fibers was 11% higher than that of the GFRP/plain beam GG, while the GFRP/FRC beams with steel fibers recorded an ultimate load that is 25% higher than that of the GFRP/plain beam. All the GFRP beams failed by concrete crushing, and a more ductile behavior was observed in the FRC beam than in the plain-GFRP beam. However, the CFRP/FRC beams failed by FRP rupture, even though they were all over-reinforced to fail by concrete crushing. This was because of the higher concrete strain of around 0.0035 that was reached by the addition of fibers. In this case, the FRP bars ruptured and the concrete did not reach its crushing strain. Cracks in the FRC beams were shorter and had a smaller width than those of the plain concrete beams and that is due to the bridging effect of the added fibers. The study also included ductility index determination based on the energy method defined by Naaman and Jeong [35], [39]. The study concluded that the ductility index of CFRP/FRC beams is smaller than the ductility index of CFRP/RC beams. This is due to the brittle failure by FRP rupture that occurred in the SFRC/CFRP beams. The ductility index of GFRP/FRC beams is 80% higher than the ductility index of GFRP/RC beams. This indicates that fibers increased the ultimate compressive strain of the concrete and thus resulted in higher plastic behavior (ductility).

The main scope of this research is to examine the flexural behavior of concrete beams reinforced with BFRP bars and cast of a concrete mix exhibiting improved properties. Initially, the mechanical properties of the concrete mixes and the FRP reinforcing bars are investigated through material evaluation. Concrete cubes, cylinders and prisms are tested under a compression test, a split tensile test and a flexure test, whereas the FRP and steel reinforcing bars are tested under a tensile test. A four-point bending test is carried out to examine the flexural behavior of fiber-reinforced concrete beams reinforced longitudinally with BFRP bars. The study includes an investigation of flexural capacity, cracking behavior, and mid-span deflection, which is achieved through the test setup and instrumentation. Lastly, an analytical evaluation of the beams' flexural performance including crack width, deflection, and load carrying capacity is performed and the results are compared with the experimental results.

Chapter 3. Experimental Program

In this chapter, the experimental program including the materials properties, specimen configuration, test setup, and design considerations and equations are discussed.

3.1. Material Properties

In this section the properties of all the materials that were used in this study are discussed. Most of these properties are based on material testing conducted in the laboratory of the AUS.

3.1.1. Basalt fiber-reinforced polymer (BFRP) bars. BFRP bars are used as a flexural reinforcement in the beams. The BFRP bars have an ultimate tensile strength of 1100 MPa and an elastic modulus of 46 GPa, as specified by the manufacturer. Different bar diameters are used in this study including 8, 10, 12 and 16 mm. The bars surface is sand coated for the purpose of increasing the bond between the bar and the concrete. Samples from the used bars are tested under a tensile load in order to obtain the actual values. Table 5 shows the result summary of the tested BFRP bars under tensile test. The BFRP bars used in this study are shown in Figure 6.

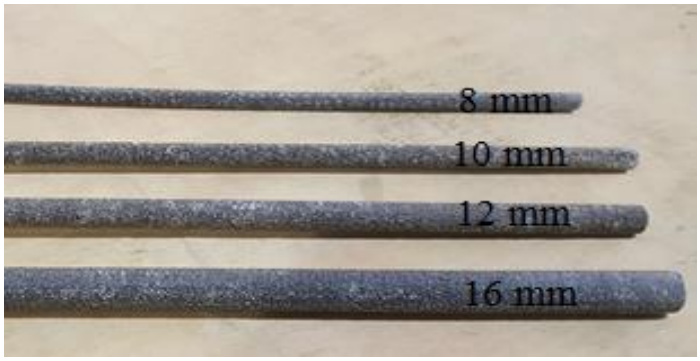

Figure 6: BFRP bars

3.1.2. Glass fiber-reinforced polymer (GFRP) bars. The GFRP bars have an ultimate tensile strength of 1000 MPa and an elastic modulus of 45 GPa as specified by the manufacturer. The bar surface is sand coated for the purpose of increasing the bond between the bar and the concrete. GFRP bars are used as a flexural reinforcement for two beams for comparison purposes. The GFRP bars used in this study are shown

in Figure 7. The mechanical properties of the GFRP bars are provided by the manufacturer and shown in Table 5.

Figure 7: GFRP bars

Table 5: Rebars properties summary

Sample designation	**Cross sectional area A (mm^2)**	**Ultimate tensile stress f_u (MPa)**	**Ultimate strain ε_u (%)**	**Modulus of elasticity E (GPa)**
BFRP 8	57.4	1075.1±37	2.5±0.1	42.9±1.4
BFRP10	85.4	1028.7±47	2.4±0.1	42.8±1.3
BFRP12	121.3	1118.6±31	2.4	46.6±1.7
BFRP16	211.9	1121.3±56	2.4	46±2.1
GFRP12*	113	1000	2.3	45

*GFRP mechanical properties as per manufacturer

3.1.3. Steel rebars. A Reinforcing steel rebars of Grade 460, which have a minimum yield strength of 460 MPa, are used in this study. Steel bars are used as a flexural reinforcement in one of the beams for comparison purposes.

3.1.4. Basalt fibers. Basalt fibers are used as the main fibers for all of the BFRP reinforced concrete beams. These fibers have an elastic modulus of 94 GPa. A dosage of 0.75% of the total concrete mix volume is used in this study and its effect is investigated throughout the testing stage. Figure 8 Shows a sample of Basalt fibers used within concrete mix. Table 6 provides the mechanical properties of the basalt as per the manufacturer.

Figure 8: Basalt fibers (12 &24 mm)

Table 6: Fibers manufacturer properties

Type of fiber	**Length (mm)**	**Specific gravity**	**Young's modulus (GPa)**
Basalt fiber	12,24	2.6	94

3.1.5. Synthetic fibers. Synthetic fibers are available in 12 or 19mm length and have an elastic modulus of 9.5 GPa as provided by the manufacturer. A dosage of 0.75% of the total concrete mix volume of 12 mm length is used in this study. Figure 9 shows a sample of synthetic fibers that is used within concrete mix. Table 7 provides the mechanical properties of the basalt as per the manufacturer.

Table 7: Synthetic fibers manufacturer properties

Type of fiber	**Length (mm)**	**Specific gravity**	**Elastic modulus (GPa)**
Synthetic fiber	12	0.91	3.5

Figure 9:Synthetic fibers (12 mm)

3.1.6. Concrete mix. The beams are cast in this study with a concrete that has a target compressive strength of 40 MPa. Four different mixes are prepared: Basalt fiber-reinforced concrete (BFRC) with 24 and 12 mm fiber length, Synthetic fiber-reinforced concrete (SFRC) with 12 mm fiber length, and plain concrete. Table 8 shows the concrete mix design for the beams. Fibers are added at a dosage of 0.75% of the total concrete mix volume. In the case of FRC, the plain concrete mix design is slightly modified by the addition of 0.75 % per volume of either Basalt or synthetic fibers. Ordinary Portland cement is used for beam casting, and a chemical admixture produced by BASF is used to improve the concrete workability during the casting procedure as shown in Figure 10(a). The beam specimens are de-molded from their formwork after 48 hours, covered by cloth sheets, and cured with water as shown in Figure 10(b). The small specimens are cured by being kept inside a water tank for 28 days. After 28 days, the concrete cylinders and cubes are tested under compression in order to evaluate the actual concrete compressive strength (f'_c). In addition, the influence of adding fibers to the concrete is investigated.

(a) (b)

Figure 10: (a) casting process of specimens, (b) curing process of the concrete specimens

Table 8: Concrete mix design

Concrete mix	Fiber content (Kg/m^3)	Unit weight (Kg/m^3)							
		Cement	Water	20mm Agg.	10mm Agg.	Washed sand	Crushed sand	Dune sand	PCE
BFRC (24mm)	19.5	390	165	502	366	-	605	340	6.55
BFRC (12mm)	19.5								
SFRC	6.9								
Plain	-								

3.1.7. Evaluating the optimum fibers dosage. Determining the optimum basalt fiber content is one of the most important concerns in this study. Different concrete trial mixes with different Basalt fiber content are cast and tested. The effect of fiber content is evaluated through 3 different fiber dosages: 0.5% 0.75% of the total concrete mix volume, and 1.8 Kg/m^3 as an optimum dosage specified by the manufacturer of the basalt fibers (Galen). The plain concrete trial mix is cast as well for comparison purposes. The evaluation is based on the compression and split tensile tests conducted on the concrete cubes and cylinders. The specimens are tested at 7 and 28 days. The test results are summarized in Table 9.

Table 9: concrete trial mix results summary

Fiber dosage	Cubes compressive strength (MPa)		Split tensile strength (MPa)
	7 days	28 days	
Plain	58	64	4.15
1.8 Kg/m^3	45.5	54	3.19
0.5%	54.3	64	3.23
0.75%	58	67	4.30

It can be seen from table 8 that specimen with 0.75% fiber dosage recorded the best results in terms of compressive strength and split tensile strength compared to plain concrete specimen. For the cubes' compression strengths, both the concrete specimen of 0.75% fiber dosage and the plain concrete specimen recorded the same values at 7 days of 58 however, at 28 days the strength of 0.75% fiber dosage specimen exceeded the strength of plain concrete one by 3 MPa. Therefore, in this study, the 0.75% of the total concrete volume is considered to be the optimum fiber dosage and is used for casting all the fiber-reinforced concrete beams.

3.1.8. Fiber-reinforced concrete. After taking 0.75% as an optimum fiber dosage in the concrete mix, the concrete compressive strength (f'_c), tensile strength, and flexural strength are measured for all the concrete mixes used in this study to investigate the influence of adding fibers at a material level. The results indicate that, for the same volumetric ratio of basalt and synthetic fibers, the addition of basalt fibers increases the concrete compressive strength, whereas the addition of synthetic fibers results in a slight decrease. Moreover, the basalt fiber-reinforced concrete specimens show a higher split tensile strength than the synthetic fiber-reinforced concrete specimens when compared to the plain concrete specimen. Most studies conducted on FRC concrete indicate that the f'$_c$ value shows a slight increase by the addition of fibers [8], [13], [15]. Table 10 summarizes the test results for all of the concrete specimens. The effect of using fibers in the concrete is also observed in the failure mode of the cube specimens as shown in Figure 11, the plain concrete cube is severely damaged compared to the basalt and synthetic fiber-reinforced specimens, which can be attributed to the bridging effect of fibers in the concrete.

Table 10: concrete specimens test results

Concrete specimen	Cubes 28-days compressive strength (MPa)	Split Tensile strength (MPa)	Modulus of rupture (MPa)
24 mm Basalt fiber	47	3.5	6.44
12 mm basalt fiber	48	3.8	8.24
Synthetic fiber	38	3.0	4.22
Plain concrete	42	2.6	3.13

(a) (b) (c)

Figure 11: Tested specimens, (a) plain concrete, (b) basalt fibers concrete, (c)synthetic fibers concrete

3.2. Beams Configuration

In the design of the cross section, the width of the beams is first determined by taking into consideration all the recommendations of the ACI codes related to number of bars, diameter of the bars, spacing between the bars, and clear concrete cover. By considering all of these values and requirements, the width of the beams is found to be 180 mm. For the beam depth, the ACI 440-1R-06 code has recommended that the minimum thickness of simply supported FRP beams be a tenth of their span length (L/10). In addition, another criterion controlling the depth of the beams is the shear span to effective depth ratio (a/d). In this study, to ensure a pure flexural behavior and bending failure for the specimens, the ratio (a/d) is taken as equal to or greater than 3 ($\frac{a}{d} \geq 3$). Therefore, the depth of the specimens is obtained to be 230 mm. The clear span of the beams is 1700 mm. However, an extension of 150 mm from each side over the support must be added to ensure enough development length during the flexure test, resulting in a total length of 2.0 m (2000 mm) for the beam specimens. Figure 12 shows the typical cross-section of the tested specimens.

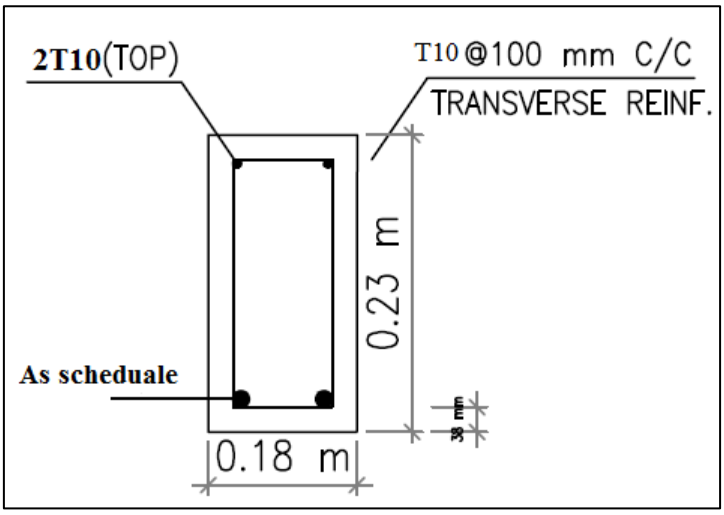

Figure 12: Beam Typical detail

3.3. Flexure Test

A number of 12 rectangular beams are prepared for testing as shown in Table 11. The experimental program is mainly based on the four-point bending test to investigate the flexural performance of the beams. The test includes many variables, namely the flexural reinforcement ratio (ρ), the type of reinforcement, and the type of the fibers. The types of flexural reinforcement in this study include BFRP, GFRP, and

steel. The study examines the flexural behavior of No. 8, 10, 12 and 16mm BFRP bars and compares it to that of No. 12 and 16 mm GFRP bars and No.12 steel bars. The concrete matrix contains beams with Basalt and synthetic fibers in addition to one plain concrete BFRP beam for comparison purposes. A beam of basalt fiber-reinforced concrete with 2No.12 BFRP is considered the controlling specimen. The beams are designated based on the type and number of longitudinal flexural reinforcement rebars and the type of fibers within the concrete mix. The first number represents the number of rebars used in each beam followed by the term T which indicates the diameter of the rebar in millimeters. Then the letter B, G, or S indicates the type of reinforcement which is BFRP, GFRP, or steel, respectively. The last term (B1, B2, S, and P) refers to Basalt of 24 mm or 12 mm length, synthetic fibers, and plain concrete, respectively. For instance, beam 2T12BB1 refers to the beam reinforced with 2 No. 12 BFRP bars and containing basalt fibers of 24 mm length.

Table 11: Test matrix

Sr #	**Beam**	**Reinf. type**	**A (mm^2)**	**ρ_f**	**Flexural stiffness EA (MN)**	**ρ_f / ρ_{fb}**	**Type of fibers**
1	2T12BB1 (Control)	BFRP	2#12=243	0.0073	11.32	2.8	Basalt[a]
2	2T16BB1	BFRP	2#16=424	0.0129	19.5	5.2	Basalt
3	2T10BB1	BFRP	2#10=171	0.0051	7.3	1.8	Basalt
4	3T10BB1	BFRP	3#10=256	0.0077	10.96	2.75	Basalt
5	3T8BB1	BFRP	3#8=172	0.0051	7.37	1.96	Basalt
6	2T12BS	BFRP	2#12=243	0.0073	11.32	2.8	Synthetic
7	2T12BP	BFRP	2#12=243	0.0073	11.32	2.8	-
8	2T12GB1	GFRP	2#12=243	0.0073	12.2	2.15	Basalt
9	2T12GB2	GFRP	2#12=243	0.0073	12.2	2.15	Basalt2[b]
10	2T12SB1	Steel	2#12=226	0.0068	45.2	0.17	Basalt
11	2T12BB2	BFRP	2#12=243	0.0073	11.32	2.8	Basalt 2
12	2T16BB2	BFRP	2#16=424	0.0129	19.5	5.2	Basalt 2

a basalt fibers with 24 mm length b basalt fibers with 12 mm length

3.4. Test Setup and Instrumentation

All the tests are conducted using a Universal Testing Machine (UTM) at the American University of Sharjah (AUS) with a 2500 KN load capacity as shown in Figure 13(a). The beams are prepared to be tested using four-point bending with the load divided equally by the means of spreader beam over a constant moment region of 500 mm. The beams are tested over a 1700 mm clear span. The load is applied using a

hydraulic jack and measured by a load cell attached above the spreader beam at mid-span. During the flexure test, two different parameters, load and midspan deflection, are measured by the testing machine. Crack width is measured using demic gages attached over the first three cracks that appear on the beams' surfaces in the flexural region. Strain gages are used to measure the strains in the concrete and reinforcement bars at mid-span. For concrete, the strain gauges are attached in the compression zone, starting at 1 cm from the top of the beam and leaving 5 cm of spacing between each two consecutive gauges. Also, three LVDTs are used to measure the deflection at quarter, half and three quarters of the beam span. Figure 13(b) shows the test setup for the beams. In addition, the specimens are continuously observed to mark the crack patterns and note any signs of distress during the loading process. Load readings are observed and written down for every crack or occurring change.

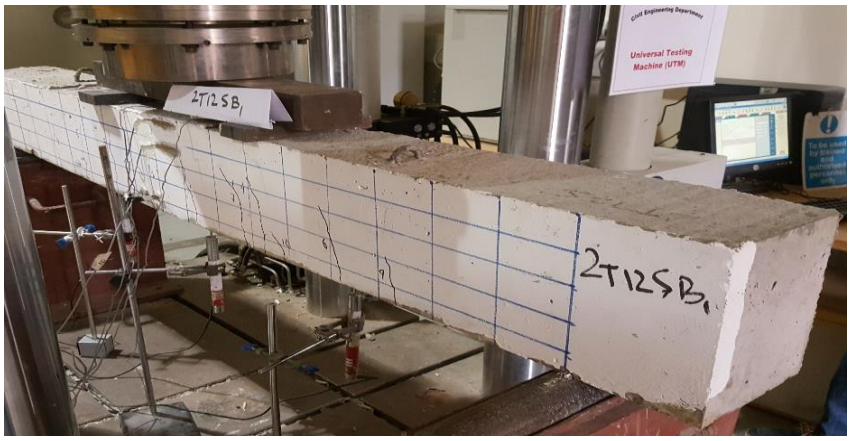

(a)

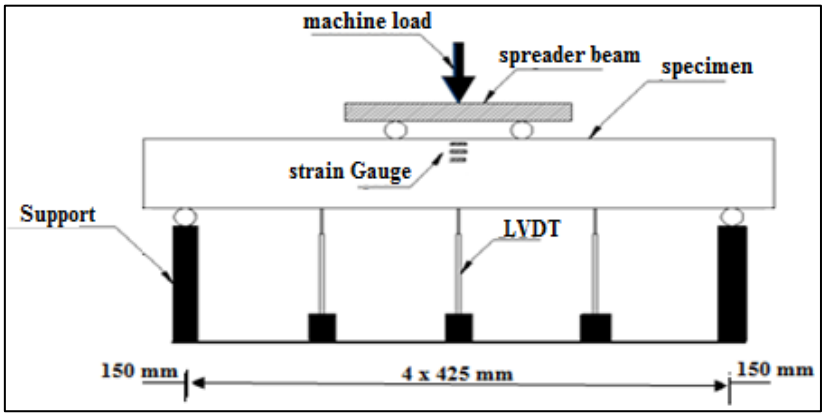

(b)

Figure 13: (a) Beam under 4-point bending test, (b)Test setup

Chapter 4. Design Considerations of Fiber-Reinforced Polymer (FRP)

In this chapter, the ACI 440-1R-06 code analytical equations are mentioned in order to predict the proposed beams' flexural behavior and compare it with the experimental results. The analysis includes a determination of flexural capacity, stress-strain curves, crack width, crack spacing, and beam deflection.

4.1. Flexural Capacity

When designing flexural beams reinforced with FRP, the American standards and design code for fiber-reinforced polymer (FRP), ACI 440-1R-06[18], allows two modes of flexural failure according to which the FRP-reinforced concrete members can be designed [16]. The first failure mode is controlled by FRP rupture, which is similar to the tension-controlled failure mode suggested by ACI-318 for steel beams. Since FRP bars have no yielding point, the precautions before failure are limited and members reinforced with these bars experience sudden and catastrophic failure. The second failure mode is controlled by concrete crushing. Although concrete is a brittle material, studies have proven that concrete structures reinforced with FRP bars experience a mode of failure of more plastic behavior than FRP rupture, and thus achieve ductile failure with more warning. Both failure modes are dependent on the FRP reinforcement ratio (ρ_f) [17]. In order to design a section that can fail by FRP rupture, the FRP reinforcement ratio should be less than the FRP balanced reinforcement ratio ($\rho_f < \rho_{fb}$). In contrast, concrete crushing failure can be accomplished by using an FRP reinforcement ratio that is greater than the FRP balanced reinforcement ratio ($\rho_f > \rho_{fb}$). Based on this phenomenon, FRP beams have been designed to be over-reinforced ($\rho_f > \rho_{fb}$) in accordance with the balanced fiber reinforcement ratio ρ_{fb}.

As a result, ACI 440-1R-06 imposes the use of a reduction factor of 0.65 for beams that are over-reinforced to fail by concrete crushing. However, beams that are under-reinforced and fail by FRP rupture exhibit lower ductility and hence show limited failure precautions. Therefore, the ACI 440-1R requires the use of a resistance factor of 0.55 in the design. Beams that do not fall in either of the two aforementioned categories are considered to be in the transition zone and their reduction factor is calculated by linear interpolation.

Although the compression failure of concrete beams is recommended, actual members may not fail as anticipated. The reason behind this is mainly due to the analytical assumptions, the variations in section geometry and reinforcement, and the uncertainties of the material properties and strengths [17]. For instance, adding fiber to the concrete mix may increase the concrete compressive strain to a value higher than the design-assumed value of 0.003, and the member may fail by FRP rupture. Therefore, due to the previously mentioned factors, the ACI 440-1R code suggests that the upper boundary of the reinforcement ratio for FRP beams be taken as $1.4\,\rho_{fb}$. As a result, all the FRP beams in this study are reinforced with a ratio that is more than $1.4\,\rho_{fb}$ to ensure a safe gap between the two different modes of failure.

All the FRP reinforced beams in this study are designed to be over-reinforced in order to provide more ductility to their behavior and to cause them to fail by concrete crushing as recommended by the ACI 440-1R-06 code. Capacity computations for the beam cross sections will be done based on the following assumptions:

• A plane section before loading remains plane after loading, which means that the strain in the FRP bars and concrete is proportional to the distance from the neutral axis.

• The concrete compressive strain has a maximum usable value of 0.003.

• The tensile strength of concrete is neglected.

• The FRP reinforcement has linear elastic tensile behavior until failure.

• The bond between the FRP reinforcement and concrete is assumed to be perfect.

Based on these assumptions, the FRP beams are designed to have a reinforcement ratio that exceeds the balanced fiber reinforcement ratio ($\rho_f > \rho_{fb}$). For the BFRP reinforced beams, the balanced reinforcement ratio, ρ_{fb}, is defined as the amount of reinforcement needed to initiate concrete crushing at the same time as tensile rupture of the flexural reinforcement [3] , and can be obtained by the following equation:

$$\rho_{fb} = 0.85\beta_1 \frac{f'_c}{f_u}\left(\frac{E_f \varepsilon_c}{E_f \varepsilon_c + f_u}\right) \quad (1)$$

where, β_1 refers to the ratio of the depth of the whitney block to the depth of the neutral axis.

f'_c : Concrete compressive strength (MPa)

f_u : Design tensile strength of FRP (MPa)

ε_c: Ultimate concrete compressive strain

E_f: Elastic modulus of FRP bar

In fact, the FRP balanced reinforcement ratio can be even less than the minimum steel reinforcement ratio. Table 12 shows some typical values for the balanced reinforcement ratio for steel and FRP for f'$_c$ of 35 MPa.

Table 12: Balanced reinforcement ratios for different FRP materials [16]

Bar type	Yield strength f_y or tensile strength f_{fu}, ksi (MPa)	Modulus of elasticity, ksi (GPa)	ρ_b or ρ_{fb}
Steel	60 (414)	29,000 (200)	0.0335
GFRP	80 (552)	6000 (41.4)	0.0078
AFRP	170 (1172)	12,000 (82.7)	0.0035
CFRP	300 (2070)	22,000 (152)	0.0020

Table 12 clearly reports that the FRP balanced reinforcement ratio (ρ_{fb}) is much lower than the steel balanced reinforcement ratio (ρ_b). In order to design a beam, the actual reinforcement ratio of the beam should be calculated and compared to the balanced reinforcement ratio to know whether the beam should be over or under-reinforced. The reinforcement ratio of a beam cross-section can be obtained from the following formula:

$$\rho_f = \frac{A_f}{bd} \tag{2}$$

where, A_f is the total area of the FRP reinforcement used in the section

b: width of the beam (mm)

d: effective depth (mm) can be calculated as follows

$$d = \text{h} - \text{clear concrete cover} - \text{stirrups diameter} - \frac{\text{flexural bar diameter}}{2} \tag{3}$$

When ($\rho_f > \rho_{fb}$), the failure of the beam is initiated by concrete crushing and the compression stress distribution of the concrete can be represented by the ACI

whitney block. The nominal flexural strength of a section can be calculated in terms of the FRP reinforcement ratio by the following equation:

$$M_n = \rho_f f_f \left(1 - 0.59\frac{\rho_f f_f}{f'_c}\right) bd^2 \quad (4)$$

where, f_f is the FRP stress at failure and can be estimated by the following equation:

$$f_f = \left(\sqrt{\frac{(E_f \varepsilon_c)^2}{4} + \frac{0.85\beta_1 f'_c}{\rho_f} E_f \varepsilon_c} - 0.5 E_f \varepsilon_c\right) \leq f_u \quad (5)$$

Alternatively, the nominal flexural strength can be obtained based on strain compatibility and force equilibrium as shown in Figure 14 below.

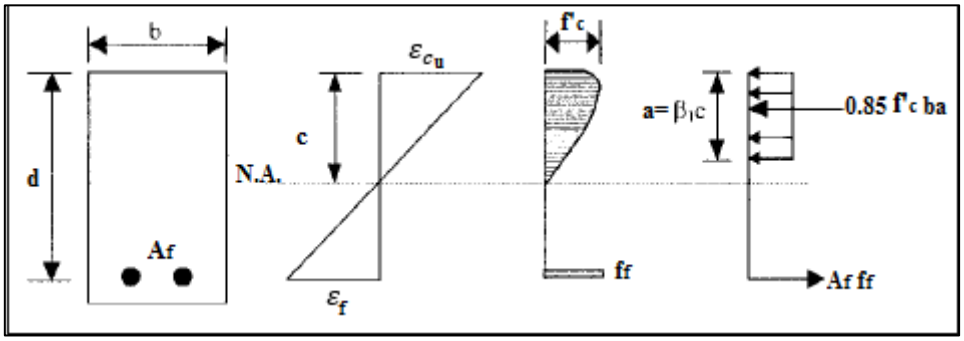

Figure 14:FRP Beam stress-strain diagram

$$M_n = A_f f_f \left(d - \frac{a}{2}\right) \quad (6)$$

$$a = \frac{A_f f_f}{0.85 f'_c b} \quad (7)$$

In the end, the ultimate applied moment should satisfy the following equation:

$$M_u \leq \varphi M_n \quad (8)$$

where the resisting factor (φ) can be obtained as shown below:

$$\varphi = \begin{cases} 0.55 \; for \; (\rho_f \leq \rho_{fb}) \\ 0.3 + 0.25\dfrac{\rho_f}{\rho_{fb}} \; for \; (\rho_{fb} < \rho_f < 1.4\,\rho_{fb}) \\ 0.65 \; for \; (\rho_f \geq 1.4\,\rho_{fb}) \end{cases} \quad (9)$$

4.2. Crack Width

Since FRP reinforcement bars have a corrosion resistance feature, the crack width limits can be relaxed for beams reinforced with FRP bars. The Canadian Standard Association (CSA 2002) permits crack widths of 0.7 mm (0.028 in) for internal exposure and 0.5 mm (0.02 in) for external exposure [17]. However, for steel reinforced concrete beams, the crack width is limited to 0.4 mm (0.016 in) [40]. For Calculating crack width, the ACI 440 code suggests the following formula:

$$w = 2\frac{f_f}{E_f}\beta K_b\sqrt{d_c^2 + (\frac{S}{2})^2} \quad \leq 0.7\ mm \tag{10}$$

$$\beta = \frac{h - kd}{d(1-k)} \tag{11}$$

$$d_c = h - d \tag{12}$$

$$s = b - 2d_c \tag{13}$$

$$f_f = \frac{M_{applied}}{A_f d(1 - \frac{k}{3})} \tag{14}$$

$$M_{applied} = \frac{Pa}{2} \tag{15}$$

$$k = \sqrt{2\rho_f n_f + (\rho_f n_f)^2} - \rho_f n_f \tag{16}$$

$$n_f = \frac{E_f}{4750\sqrt{f'_c}} \tag{17}$$

where

w= maximum crack width (mm)

f_f= FRP reinforcement stress (MPa)

E_f= FRP modulus of elasticity (MPa)

β= ratio of the distance between the neutral axis and tension face to the distance between the neutral axis and centroid of reinforcement

d_c= concrete cover from tension face to the center of closest bar (mm)

s= spacing between bars (mm)

K_b= FRP bond coefficient, taken as 0.6 for sand coated bar and 1.4 for ripped surface bars

P= applied load measured by the load cell (N)

a= distance between half of the load and the support (mm)

d= effective depth of the beam section (mm)

4.3. Crack Spacing

For calculating the average crack spacing of the FRP-reinforced concrete beams, the ACI 440-1R-06 code suggests the following formula:

$$S_m = 2K_b\sqrt{d_c^2 + \frac{S^2}{2}} \tag{18}$$

On the other hand, the ACI 318 code recommends the following equation for estimating the average crack spacing of steel-reinforced concrete beams:

$$S_m = 50 + 0.25k_1k_2\frac{d_b}{\rho_t} \tag{19}$$

where

S_m= average crack spacing (mm)

K_b= bond coefficient (ACI 440 suggests 1.4 for deformed FRP bars)

d_c= concrete cover measured from the extreme tension fiber to the center of the closest layer of longitudinal bars (mm)

S= spacing between longitudinal bars (mm)

K_1 = 0.8 for high-bond bars and 1.6 for plain bars and, k_2 = 0.5 for bending and 1.0 for pure tension.

d_b= longitudinal bar diameter (mm)

ρ_t=effective reinforcement ratio= A_s/A_{ct}

A_{ct}=effective concrete area surrounding the longitudinal tension reinforcement at a depth equal to 2.5 times the distance from the tensile face of the concrete section to the centroid of the reinforcement.

4.4. BFRP-Reinforced Concrete Beam Deflection

Based on ACI 440-1R-06 code, the deflection of the beam can be calculated using the following equations:

$$\Delta_i = \frac{Pa}{24E_c(I_e)}(3l^2 - 4a^2) \tag{20}$$

$$I_e = (\frac{M_{cr}}{M_{Applied}})^3 \beta_d I_g + \left[1 - (\frac{M_{cr}}{M_{Applied}})^3\right] I_{cr} \leq \quad I_g \tag{21}$$

$$\beta_d = \frac{1}{5}\left(\frac{\rho_f}{\rho_{fb}}\right) \leq 1 \tag{22}$$

$$I_{cr} = \frac{bd^3}{3}k^3 + n_f A_f d^2(1-k)^2 \tag{23}$$

$$M_{cr} = \frac{2f_r I_g}{h} \tag{24}$$

$$f_r = 0.62\sqrt{f'_c} \tag{25}$$

$$I_g = \frac{bh^3}{12} \tag{26}$$

where

$M_{applied}$= moment due to applied load (N.mm)

l= span length (mm)

E_c= concrete modulus of elasticity (MPa)

I_e= effective moment of inertia (mm^4)

I_{cr}= moment of inertia of cracked section (mm^4)

β_d= reduction factor related to the reduced tension stiffening of FRP beams

I_g= gross moment of inertia for the section (mm^4)

ρ_f= FRP reinforcement ratio

ρ_{fb}= FRP balanced reinforcement ratio

f_r= FRP stress of cracked section (MPa)

h= depth of the beam (mm)

b= width of the beam (mm)

Chapter 5. Experimental Results

5.1. Load VS Midspan Deflection

The Load versus midspan deflection response of all the twelve beams is plotted as shown in Figure 15. The beams are grouped based on the proposed study parameters. The maximum measured values for loads, moment capacities, and mid-span deflections; first cracking loads, curvature ductility, and failure mode for all the 12 beams are given in Table 13.

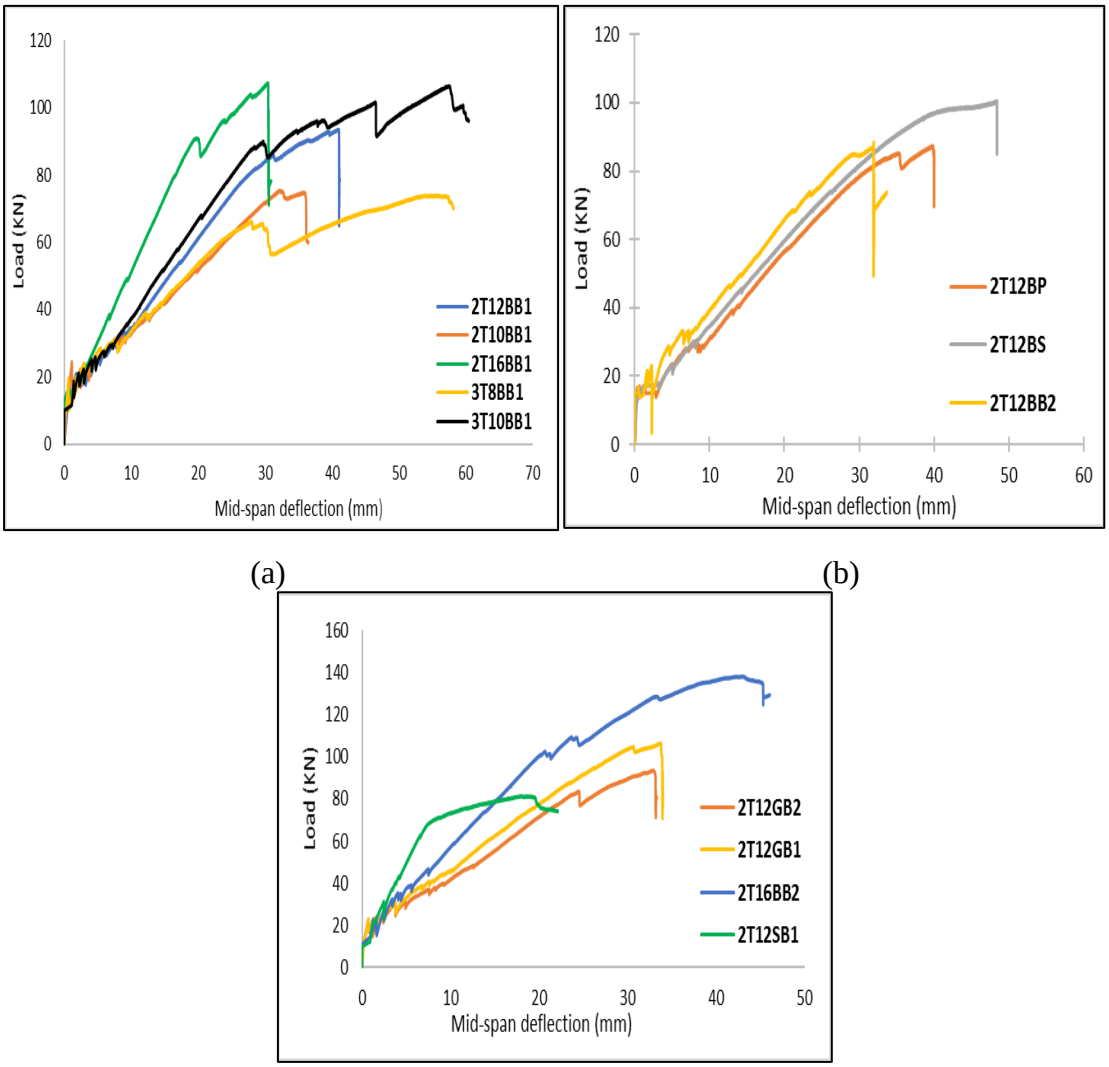

Figure 15: experimental Load vs Mid-span deflection for tested beams: (a) different reinforcement ratios; (b) different fibers type; (c) different reinforcement types

Table 13: Summary of flexural test results

Beam	Max.Load (KN)	Nominal Moment capacity (KN.m)	Max. Mid-span deflection (mm)	First cracking Load (KN)	Curvature ductility (unitless)	Failure mode
2T12BB1	94	28.2	43	17	2.8	Concrete crushing
2T10BB1	76	23	39	13	1.4	Concrete crushing
2T16BB1	108	32.4	32	23	1.9	Concrete crushing
3T10BB1	101	30	61	18	3.5	Concrete crushing & bar rupture
3T8BB1	74	22.2	60	13	2.7	Concrete crushing & bar rupture
2T12BS	100	30	50	14	2.9	Shear compression
2T12BP	84	25.2	40	16	1.2	Concrete crushing
2T12GB1	105	32	36	17	1.9	Concrete crushing
2T12GB2	94	28.2	35	17	1.4	Concrete crushing
2T12SB1	82	24.6	23	24	3.5	Steel yielding
2T12BB2	88	26.4	35	15	N/A*	Concrete crushing
2T16BB2	138	41.4	47	18	2.9	Concrete crushing

*Due to the damage of concrete strain gauge

In Table 13, the curvature ductility is defined as the ratio of the curvature at the ultimate load to the curvature at 0.001 concrete strain, which is considered the beginning strain of inelastic deformations in the reinforced concrete section [13]. The curvature is estimated using the section strain distribution, which is obtained based on a linear connection between the concrete and the reinforcement strain gauges at the two cross-section extremes.

5.2. Crack Behavior

In this section the cracking behavior including, crack spacing, crack pattern and crack width are discussed for all the tested beams.

5.2.1. Crack pattern. During the flexural test, the crack behavior of all of the tested beams is monitored at different loading stages including the initiation of the first crack, the service load, and the ultimate load. Crack pattern, crack spacing, and crack width are all captured at the aforementioned stages. Figure 16 shows the crack patterns for the tested beams at the service load stage, while Figure 17 shows the propagation of the cracks at the ultimate load stages. Moreover, the loads at which each crack developed are also monitored, as given in Table 14. All the beam groups are compared to each other based on the proposed research objectives and are discussed in the next section.

Table 14: Cracking loads

Sr #	Beam	Crack number									
		1	2	3	4	5	6	7	8	9	10
		Load for each crack (KN)									
1	2T12BB1	16	21	22	23	24	26	27	30	33	35
2	2T16BB1	23	25	28	30	34	38	40	50	54	56
3	2T10BB1	13	18	20	30	31	32	33	38	39	39
4	3T10BB1	18	21	22	24	26	28	29	31	43	45
5	3T8BB1	10	17	20	27	30	31	32	33	38	41
6	2T12BS	12	18	20	22	24	28	30	31	32	33
7	2T12BP	9	10	12	13	17	20	28	32	37	41
8	2T12GB1	17	23	24	26	38	40	43	44	46	50
9	2T12GB2	17	24	27	30	31	31	37	38	39	49
10	2T12SB1	24	32	39	41	47	51	57	63	70	71
11	2T12BB2	20	21	22	28	33	33	34	39	47	48
12	2T16BB2	20	31	34	35	37	43	44	45	60	62

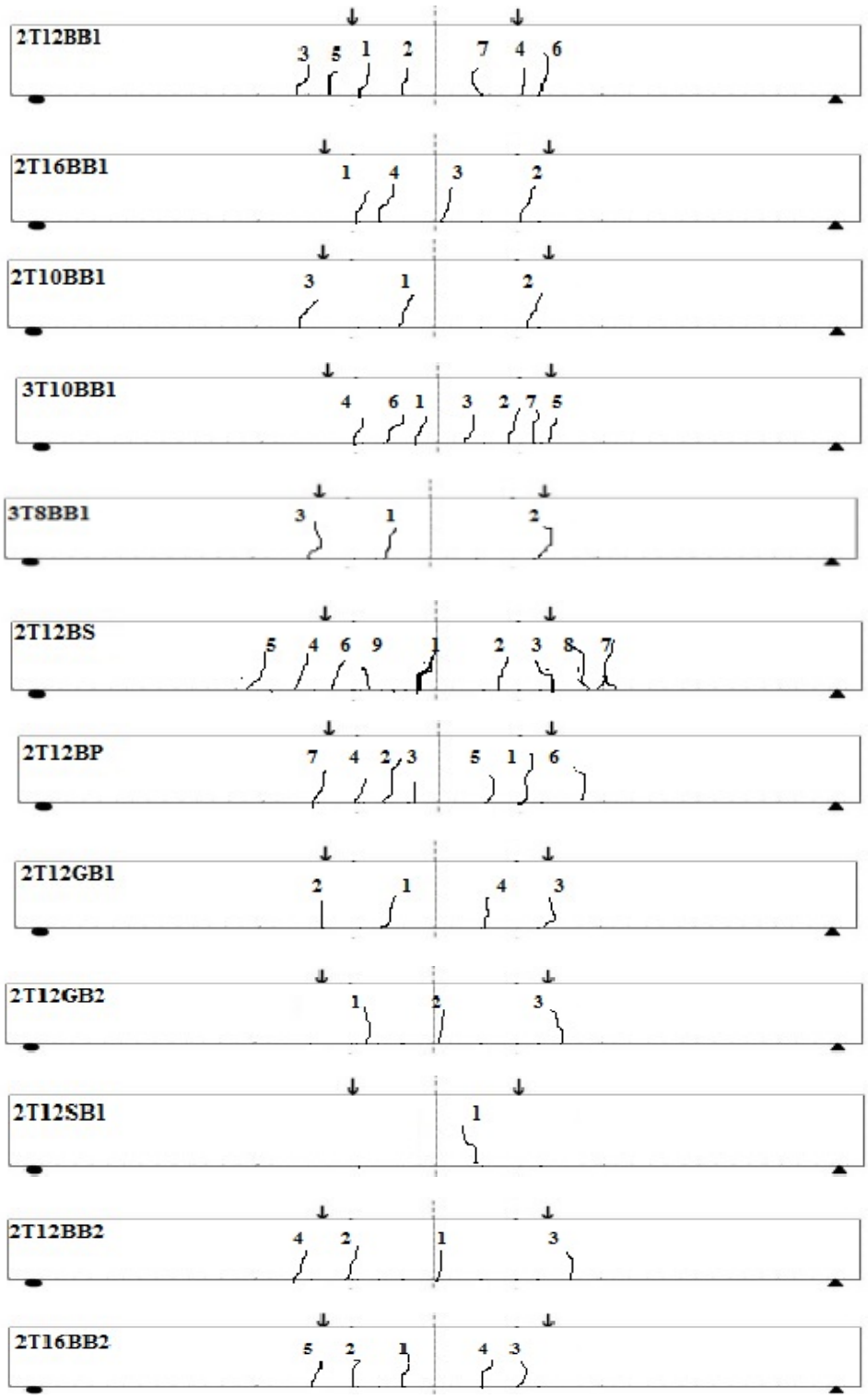

Figure 16: Crack pattern at service load stage

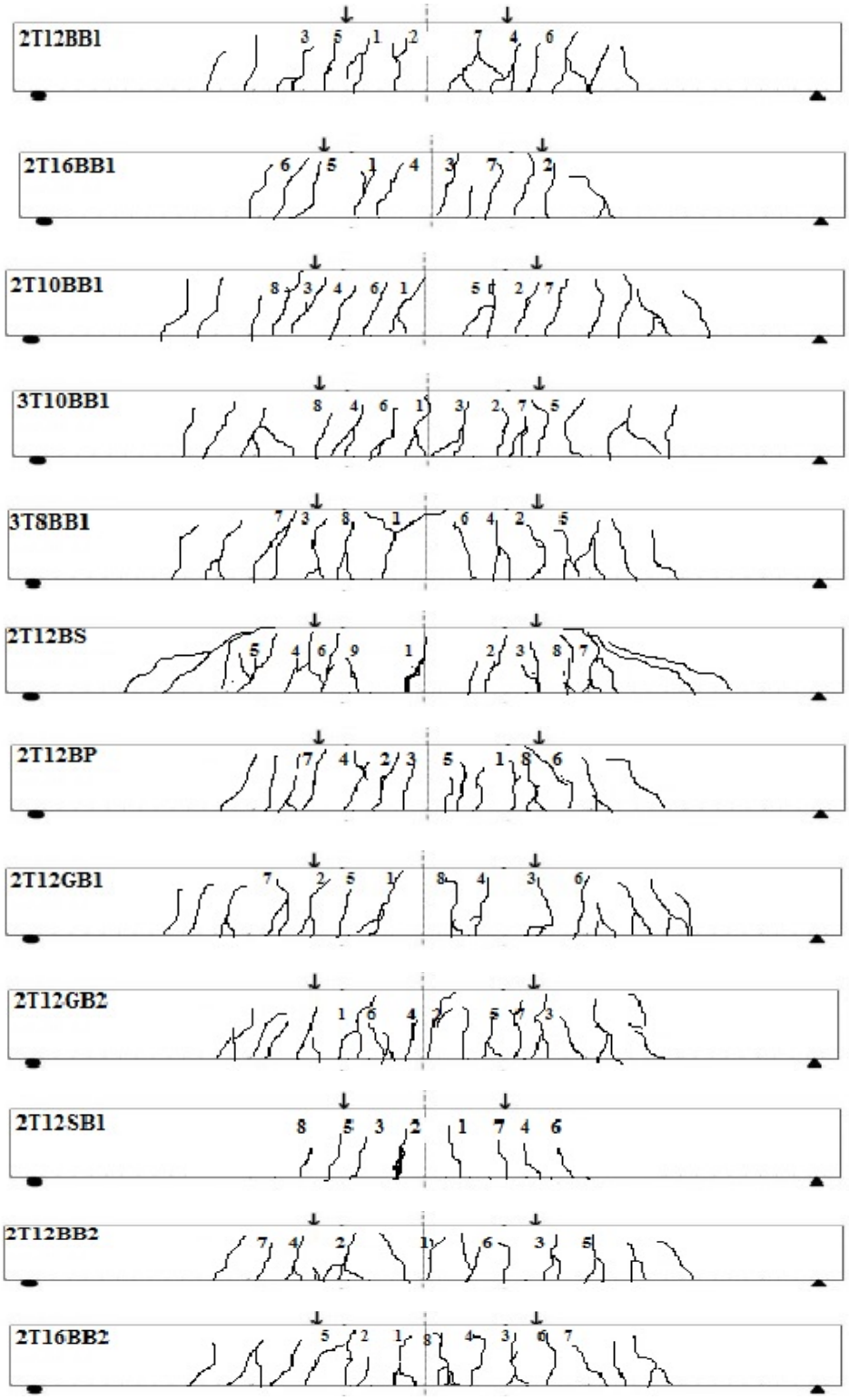

Figure 17: Crack pattern at ultimate load

5.2.2. Crack spacing. The average crack spacing at the extreme tension face for all of the tested beams is monitored and measured with the help of the grading mesh drawn on the surface of the beams. Crack spacing is a very important parameter to be captured as it helps determine the crack distribution along the pure flexure region in the beam. Table 15 gives the experimental and analytical crack spacing for the tested beams. The analytical predictions are discussed later in Chapter 6.

Table 15: Experimental and predicted crack spacing

Sr #	Beam	crack spacing mm (Exp)	crack spacing mm (pred.)		
			ACI (kb=1)	ACI (kb=1.4)	CIB
1	2T12BB1	98	102	143	148
2	2T16BB1	102	104	146	128
3	2T10BB1	92	100	141	163
4	3T10BB1	90	93	130	126
5	3T8BB1	88	91	128	138
6	2T12BS	90	102	143	148
7	2T12BP	79	102	143	148
8	2T12GB1	96	102	143	148
9	2T12GB2	80	102	143	148
10	2T12SB1	103	155		
11	2T12BB2	97	102	143	148
12	2T16BB2	99	104	146	128

5.2.3 Crack width. Crack width versus load response is plotted as shown in Figure 18. Also, the crack width of all the tested beams is monitored and measured at the longitudinal reinforcement level at different loading stages including the initiation of the first crack, the service load, and the ultimate load as given in Table 16. The theoretical crack width was calculated based on the Canadian Standard Association (CSA) with a kb factor of 0.8 and the American concrete Institution (ACI 440) with kb factor of 1 and 1.4.

The initial crack width is measured using a microscope for all the tested beams.

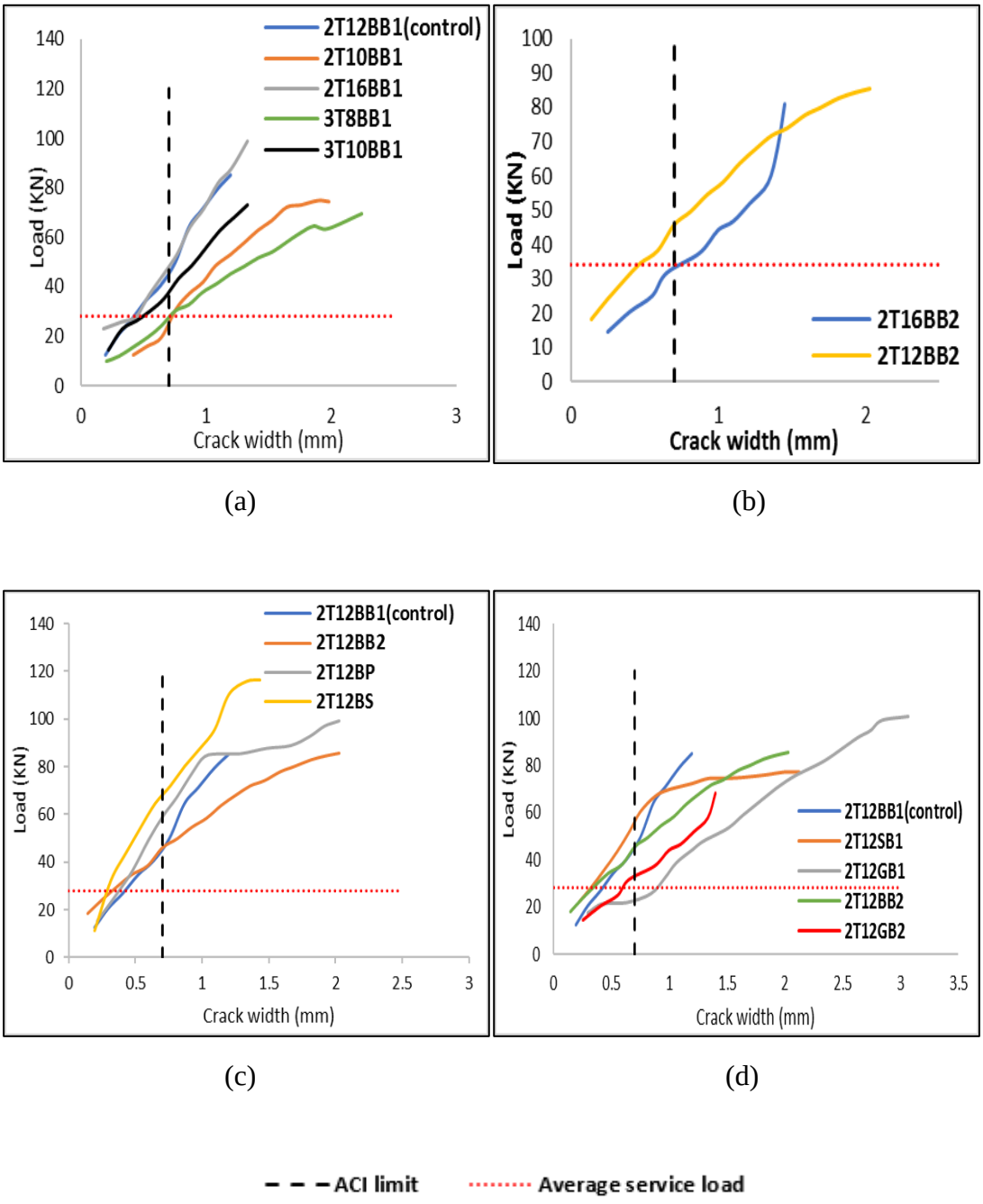

Figure 18: experimental crack width for tested beams: (a) different reinforcement ratios (24 mm basalt fibers); (b) different reinforcement ratio (12 mm basalt fibers); (c) different fiber type; (d) Different reinforcement type

Table 16: Experimental and analytical crack width

Sr #	Beam	W_{exp} (mm)		W_{pred} (0.3 Mu) (mm)		
		initial	0.3Mu	ACI (kb=1)	ACI (kb=1.4)	CSA (kb=0.8)
1	2T12BB1	0.2	0.31	0.42	0.59	0.34
2	2T16BB1	0.18	0.44	0.48	0.68	0.39
3	2T10BB1	0.42	0.53	0.35	0.50	0.28
4	3T10BB1	0.22	0.44	0.45	0.63	0.36
5	3T8BB1	0.2	0.42	0.48	0.67	0.38
6	2T12BS	0.2	0.32	0.34	0.48	0.27
7	2T12BP	0.22	0.37	0.41	0.58	0.33
8	2T12GB1	0.3	0.85	0.40	0.56	0.32
9	2T12GB2	0.23	0.45	0.39	0.55	0.31
10	2T12SB1	0.2	0.22	0.15	0.21	0.12
11	2T12BB2	0.19	0.26	0.36	0.51	0.29
12	2T16BB2	0.19	0.63	0.27	0.38	0.22

5.3. Strains at the Top Fibers of the Concrete and the Longitudinal Bars

The strain of the concrete at the top fibers of the beams and longitudinal reinforcement were captured using strain gauges at mid-span. The strain values for all the tested beams are summarized in Table 17. Moreover, Figure 19 shows the load versus strain values for the concrete at a 10 mm distance from the extreme compression fiber of the beams and for the longitudinal reinforcement.

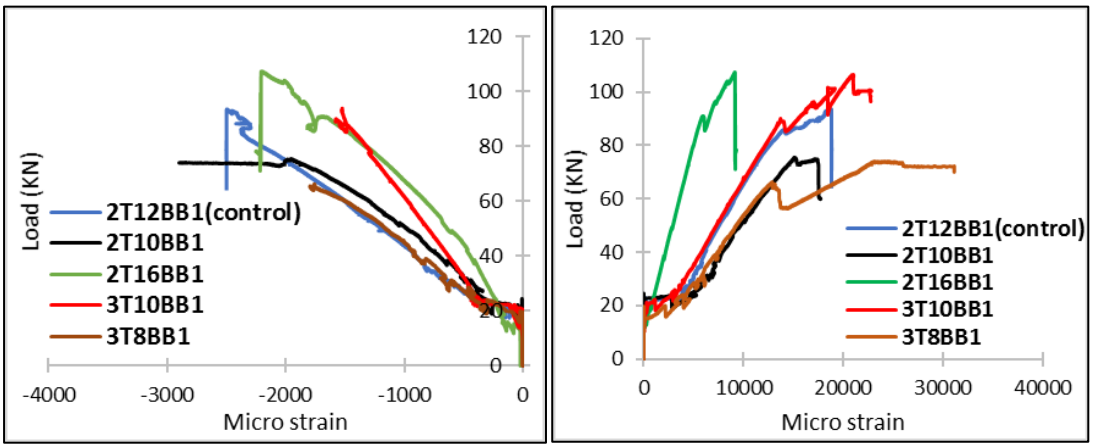

(a)

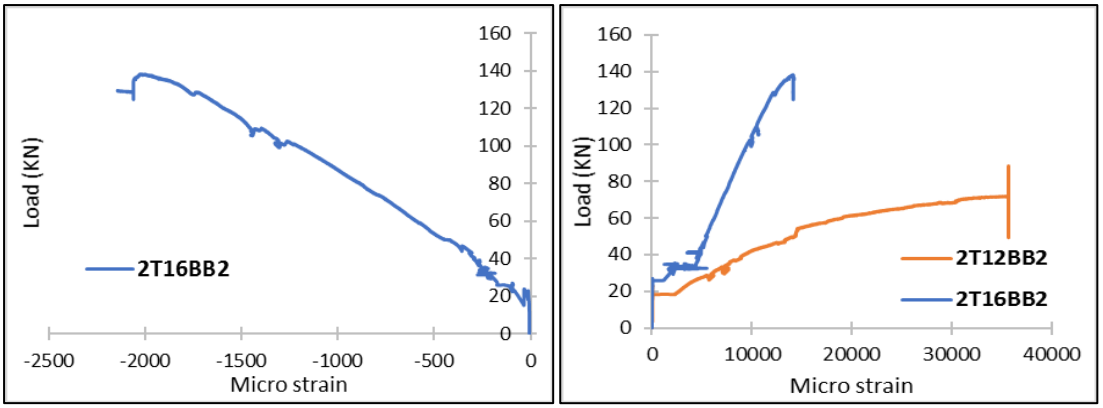

(b)

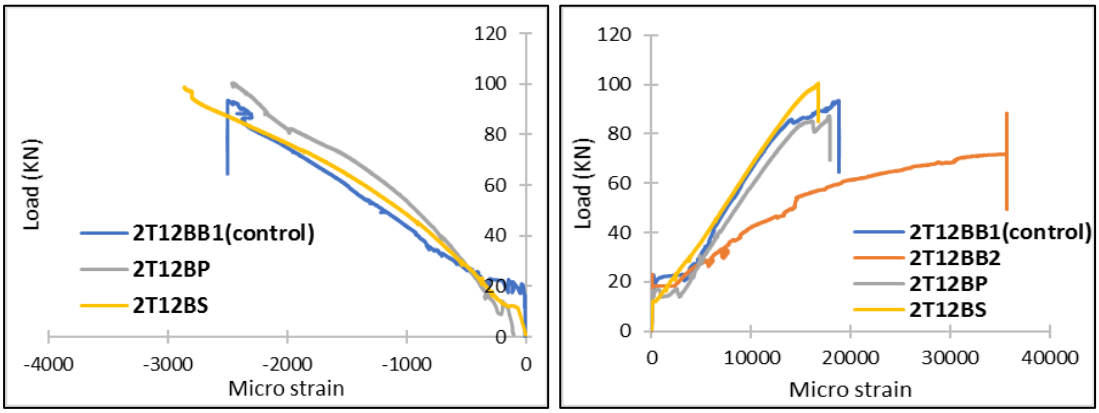

(c)

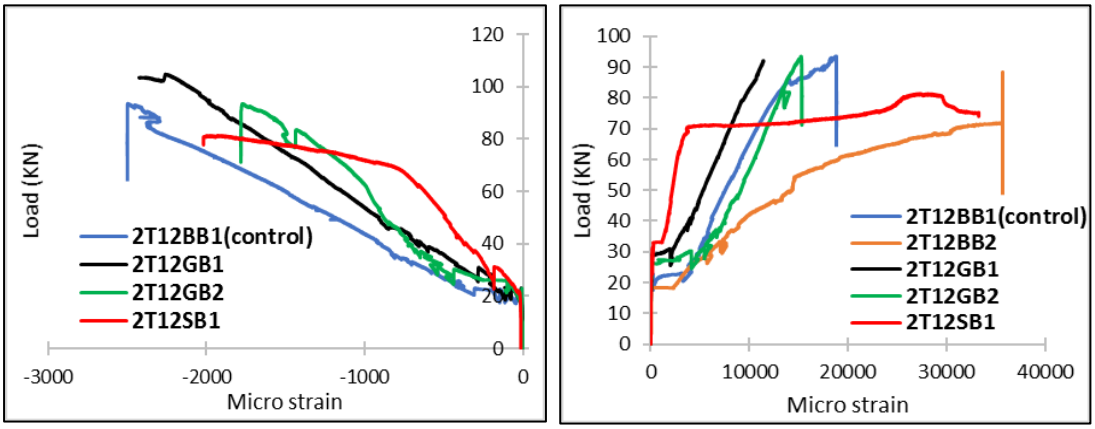

(d)

Figure 19: load vs reinforcement and concrete-strain values, (a) different reinforcement ratio (24mm basalt fibers), (b) different reinforcement ratio (12mm basalt fibers); (c) different fibers type; (d) different reinforcement type

Table 17: concrete and reinforcement strain

Beam	**Load**	**Concrete strain**	**Longitudinal reinforcement strain**
2T12BB1	94	0.0037	0.0188
2T10BB1	76	0.0034	0.0174
2T16BB1	108	0.0032	0.010
3T10BB1	101	0.0029	0.0230
3T8BB1	74	0.0031	0.0232
2T12BB2	100	N/A*	0.0220
2T16BB2	84	0.0031	0.0140
2T12GB1	105	0.0032	0.0114
2T12GB2	94	0.0027	0.0152
2T12SB1	82	0.0037	0.0280
2T12BS	88	0.0041	0.0195
2T12BP	138	0.0031	0.0130

*Due to the damage of concrete strain gauge

Chapter 6. Discussion of Results

In this chapter, the results of the experimental program for all specimens are discussed in terms of load versus mid-span deflection responses, modes of failure, and cracks behavior. The discussion and analysis of the results, including the effect of using different reinforcement ratios, different types of fibers, and different reinforcement bar materials, will be presented as well.

6.1. The Effect of Reinforcement Ratio (ρ)

The effect of the reinforcement ratio on the load versus mid-span deflection behavior is observed with the use of different reinforcement ratios. The flexural capacity increases by increasing the reinforcement ratio as shown in Figure 20. The increase was not proportional, which supported the ACI 440-1R-06 code equation for predicting the flexural capacity. The percentage increase is found to be 23% for a 43% increase in the reinforcement ratio between beam 2T10BB1 and 2T12BB1 and 15% for 77% increase in the reinforcement ratio between 2T12BB1 and 2T16BB1.

The cracking moment of the beams ranged from 4 to 7 kN.m with an average of 5.5 kN.m. This value is approximately 19% of the average ultimate moment capacity. Although the controlling variable for predicting the cracking moment is modulus of rupture, increasing the reinforcement ratio increased the cracking moment for the tested beams, which may be attributed to the higher contribution of the BFRP bars on carrying the loads as the reinforcement ratio increased. Similar behavior reported by Benmokrane et al [41].

On the other hand, there is no significant effect on flexural capacity observed by increasing the number of rebars. However, for almost the same stiffness and reinforcement ratio, the beam with 3 BFRP bars (3T10BB1) showed a much higher ductility than the one with 2 BFRP bars (2T12BB1) as shown in Figure 15(a). The same behavior was observed for beams 2T10BB1 and 3T8BB1. This was due to the increased concrete ultimate strain for the beams with 3 bars which allowed the BFRP bars to contribute more in carrying the load and therefore achieve higher bar strain which resulted in sustaining more loads with higher deflection.

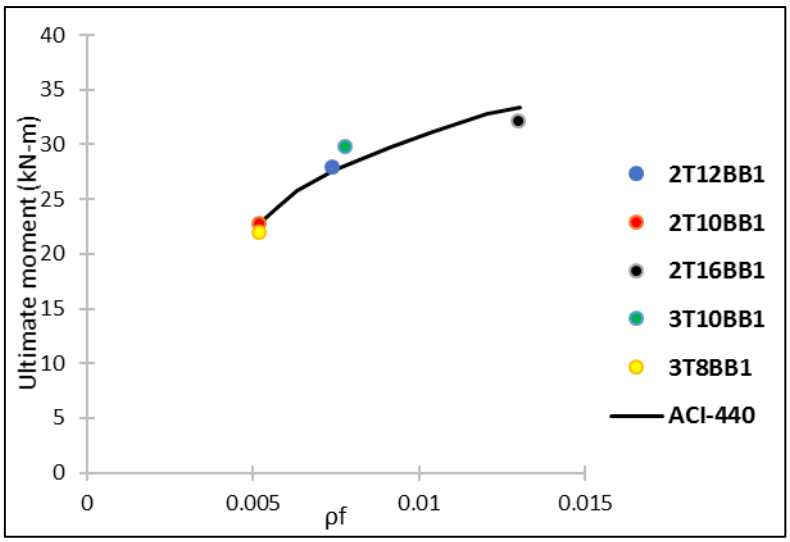

Figure 20: Ultimate moment vs reinforcement ratio

Regardless of the reinforcement ratio, all beams showe the same pre-cracking stiffness behavior until the first cracking load. After the first crack, the flexural stiffness of the beams was significantly reduced as shown in Figure 21 (a). As expected, the BFRP bars showed a linear elastic behavior until failure (concrete crushing). The same thing was reported by Wang et al. [13]. Similarly, beam 2T16BB2 exhibits a higher stiffness than beam 2T12BB2 for the 12 mm basalt fiber-reinforced concrete beams as shown in Figure 21(b).

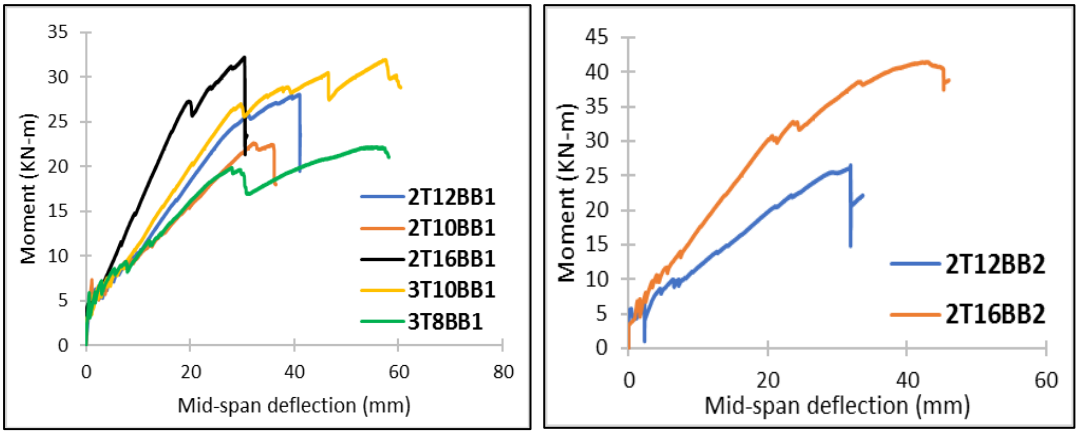

(a) (b)

Figure 21: Moment vs mid-span deflection for different reinforcement ratio; (a) 24mm basalt fiber-RC beams; (b)12mm basalt fiber-RC beams

The tensile strain in the rebars is almost the same for beams 2T12BB1 and 2T10BB1, whereas beam 2T16BB1 showed significantly lower strain in the bars as shown in Table 17. Generally, the beams with lower reinforcement ratios show a sharp increase in the reinforcement strain as illustrated in Figure 19(a &b). This can be attributed to the sudden change in the beams' stiffness at cracking. The same thing is reported for different FRP bar reinforced concrete beams [41]–[43].

Moreover, it can be observed that increasing the reinforcement ratio of the tested beams has a significant effect on the cracking pattern at the service and ultimate loads as shown in Figure 16 and Figure 17. The propagation of cracks in the tested beams follows the traditional flexural-crack pattern. Cracks start at the pure flexure region in the tension face then propagate gradually towards the compression face where the concrete crushing occurs. The crack spacing is proportional to the reinforcement ratio as shown in Table 15. The crack width follows almost the same trend for beams 2T12BB1 and 2T16BB1, whereas beam 2T10BB1 shows wider cracks as the load propagates, which can be seen by the steeper curve in Figure 18(a). This can be attributed to the higher contribution of the BFRP bars on carrying the loads as the reinforcement ratio increased. The same conclusion can be drawn for beams 2T12BB2 and 2T16BB2 with different reinforcement ratios but contain 12 mm length basalt fibers as shown in Figure 18(b).

Figure 22(a-e) shows the failure mode of the aforementioned beams, where concrete crushing is the main mode of failure for all of them. In addition, it can be clearly seen from Figure 22 (f-g) how beams 3T10BB1 and 3T8BB1 both failed by concrete crushing and BFRP bar rupture. The concrete crushing occurred first. Then, due to the increasing concrete strain, the beams continued to bear the applied load but in lower increments, and the BFRP bars exhibited high stresses and achieve higher strain until it reached the rupture strain where the bars failed by ruptured as well. This failure mode can be clearly noticed in the load versus mid-span deflection curves (Figure 15(a)), where after the first drop occurs due to the concrete crushing, the load starts increasing again.

(a)

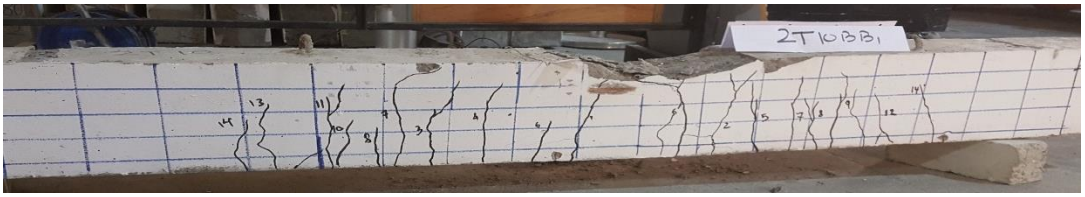

(b)

(c)

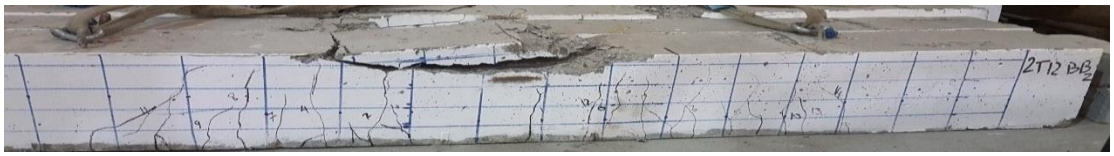

(d)

(e)

(f)

Figure 22: Failure mode of different reinforcement ratios, (a-c) basalt fiber of 24 mm length, (d-e) basalt fibers of 12 mm length; (f) 3-BFRP bars

6.2. Effect of Fibers

The effect of using fibers within the concrete mix is captured by comparing the flexural behavior of the fiber-reinforced concrete beams with that of the plain concrete specimen. The comparisons show that the addition of the basalt and synthetic fibers showed a slight improvement in the load carrying capacity and improves both the cracking and post-cracking behavior of the reinforced-concrete beams with the same reinforcement ratio as shown in Figure 23.

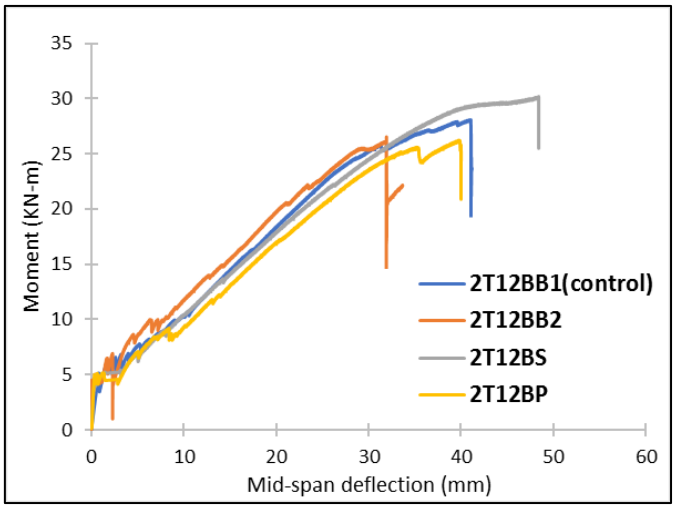

Figure 23: Moment vs mid-span deflection for different fiber type

The basalt fiber-reinforced concrete beam 2T12BB1, which contains fibers of 24 mm length, provides a higher moment capacity than beam 2T12BB2, which contains fibers of 12 mm length. The percentage increase is found to be 12% and 5% for beams 2T12BB1 and 2T12BB2, respectively, compared with the plain concrete specimen 2T12BP. The highest increasing percentage is found at 19% in the synthetic fiber-reinforced concrete beam 2T12BS (see Table 13). Although synthetic fibers have a lower tensile strength than basalt fibers, they have a higher contribution to the load capacity. This can be attributed to the lower modulus of elasticity of the synthetic fibers compared to basalt fibers, resulting in rupture strain for the synthetic fibers that is much higher than basalt fibers. Hence, the fiber rupture strain will be higher than the ultimate tensile strain of concrete at failure. Therefore, the FRC concrete beams will crack way before the fiber strength is reached. Due to this phenomenon the synthetic FRC beam was capable of sustaining more load with higher deflection. The same behavior was reported by Wang et al [13].

Moreover, the addition of fibers to the concrete helps control the compression failure of the fiber-reinforced concrete beams by the means of the fiber bridging effect, allowing the high strength of the FRP reinforcement to be utilized more. This can be considered the main reason for the increase in flexural capacity noticed in the fiber-reinforced beams. For instance, the ultimate concrete compression strain near the top extreme of the mid-span is found to be 0.0037 for beam 2T12BB1. Synthetic fiber-reinforced beam 2T12BS record the highest concrete strain value of 0.0041 compared with plain concrete beam 2T12BP's strain value of 0.0031 as shown in Table 17. Note that, for beam 2T12BB2, the concrete strain gauge was damaged and strain values were not available.

The curvature ductility enhancement due to addition of fibers in all the fiber-reinforced concrete beams are shown in Figure 24. Introducing fibers to the concrete mix improves the brittle behavior of the BFRP bars. The basalt fiber-RC beam 2T12BB1 recorded lower ductility than synthetic fiber-RC beam 2T12BS. The plain concrete beam 2T12BP had the lowest ductility as expected (see Table 13). As mentioned previously, this increase in the curvature ductility allows the beams to utilize the high tensile strength of the BFRP bars, and therefore sustain more loads with controlled deflection. The same behavior for the synthetic fiber RC beams reported by Yang et al.[15].

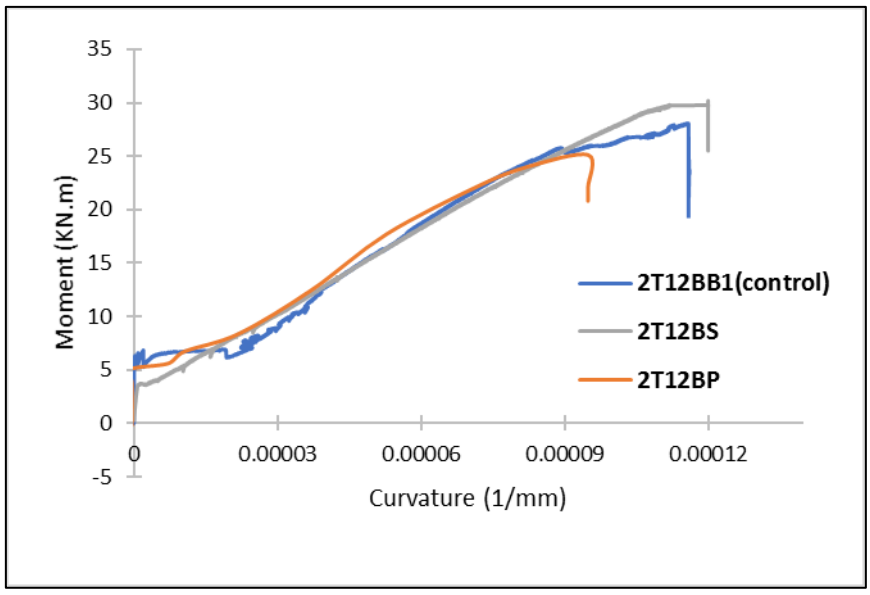

Figure 24: moment vs curvature response for different fibers type

Basalt and synthetic fibers help control the propagation of the cracks towards the compression fiber, and therefore the failure in beams containing these fibers is less severe than in the plain concrete beam as shown in Figure 25. It can be seen from the figure how beam 2T12BP failed with larger damaged area compared to the fiber-reinforced concrete beams. On the other hand, beam 2T12BS with synthetic fibers failed in the shear compression failure mode. The pure flexural cracks in the shear span bend gradually towards the loading points. The vertical flexural cracks in the shear span gradually bend towards the load points as the load increases and become inclined shear cracks. These cracks propagate deeper in the beam and become weak points; therefore, with the increasing load, the cracks open and the failure occurs. The same shear compression failure was reported by other researchers [8], [15], [39], [44], [45].

The influence of using fibers on the cracking behavior was mainly observed through its capability of closing the cracks and restraining its propagation (bridging effect) in the fiber-reinforced concrete beams. The fiber-reinforced concrete beams show higher first cracking loads than the plain reinforced concrete beam. Basalt and Synthetic fiber-reinforced beams 2T12BB1 and 2T12BS record the highest first cracking load of 17 KN, followed by 15 kN and 14 kN for beams 2T12BB2 and 2T12BP, respectively, as shown in Table 13.

Moreover, the effect of adding fibers to the concrete is observed through the propagation of cracks at the top of the beams as shown in Figure 16 and Figure 17. At the service load, which is considered to be at 30% of the nominal capacity, the number of cracks increases in 2T12BS but decreases in 2T12BB2 compared with the plain concrete beam. The same number of cracks appears in beam 2T12BB1 as shown in Table 14. The effect of basalt fiber in controlling the number of cracks at the service loading stage is slightly better than that of synthetic fiber.

At the ultimate loading stage, although the number of cracks is more in the fiber-reinforced concrete beams, the depth of these cracks is considerably lower than the depth of the cracks in the plain concrete beam. The synthetic fiber-reinforced beam is an exception as it has the same crack depths (Figure 17). In general, this indicates that the bridging effect helps control and restrain crack depth and propagation in the fiber-reinforced concrete beams.

(a)

(b)

(c)

(d)

Figure 25: failure mode of different fibers reinforced concrete beams, (a) Basalt fibers (24 mm), (b) basalt fibers (12 mm), (c) plain concrete, (d) synthetic fibers

The effect of fibers on crack width is investigated by monitoring the widths of the first three cracks that appear in the constant flexure moment region of specimens. Table 16 shows crack widths of the tested beams in three various stages: initial crack width, service load crack width, and ultimate stage crack width. It can be seen from Figure 18(c) that the basalt fibers have no potential of restraining the crack width propagation at the service load stage, whereas the synthetic fibers improve the cracking behavior. The effect of adding fibers to the concrete is mostly significant in the case of beams 2T12BB1 and 2T12BS at the late loading stage and prior to failure, where the increase in the crack width with the load is slow compared with the other specimens,

2T12BP and 2T12BB2. The plain concrete beam exhibits a sudden crack width increase after the load of 82 kN. This may be attributed to the absence of the bridging effect with the increasing stresses in the concrete. The beam with basalt fibers of 12mm length, 2T12B2, shows little bridging in its cracks compared to the beam with basalt fibers of 24mm length which shows a considerable increase in crack width after the service loading stage. This means that a larger fiber length enhances the fiber strength and increases its ability to bridge flexural cracks in the fiber-reinforced concrete beam sections. The same results can be seen in Table 16 for the crack widths at different loading stages for all of the tested beams.

6.3 Effect of Flexural Reinforcement Type

The effect of using different types of longitudinal reinforcement on the moment versus mid-span deflection behavior is examined through a comparison of the use of BFRP and GFRP bars with the use of normal steel. Generally, the use of FRP as flexural reinforcement results in a higher moment capacity than the use of steel as shown in Figure 26. The percentage increase in flexural capacity is found to be 15% and 28% for 2T12BB1 and 2T12GB1, respectively, compared to 2T12SB1 as shown in Table 13. Regardless of the flexural reinforcement material, all the beams show the same behavior in terms of pre-cracking stiffness until the first crack load

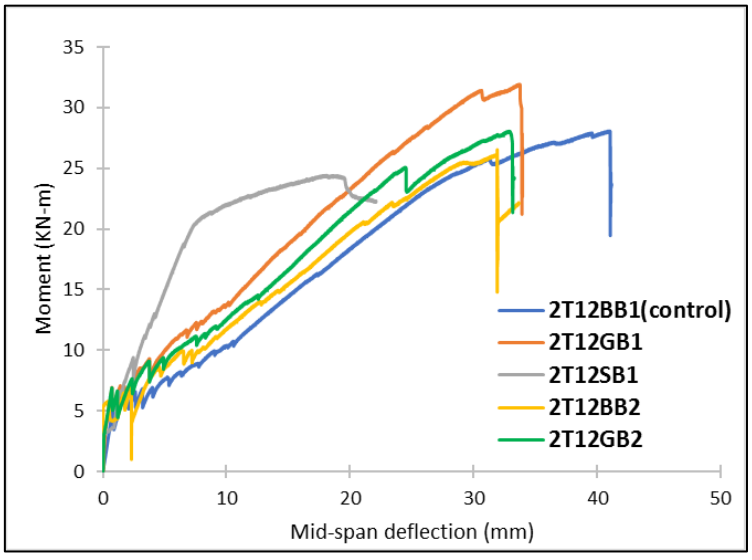

Figure 26: Moment vs mid-span deflection for different reinforcement type

The first crack moment is higher for the normal steel reinforced concrete beam than for the basalt and glass fiber-reinforced beams. After the first crack, the beam with

the normal steel reinforcement, 2T12SB1, shows a much higher stiffness than 2T12BB1 and 2T12GB1 as shown in Figure 15(c). This behavior is expected due to the low elastic modulus of the FRP bars. Table 17 provides the strain values at the two beams' cross-sectional extremes at the ultimate load. The concrete compression strain at the top of the flexural region (mid-span) is found to be 0.0037 for both BFRP-RC beam compared to 0.0032 for the GFRP-RC beam. This may be attributed to the higher deflection of the BFRP-RC beam compared to the steel and GFRP-RC beams. The same behavior is observed in the beams with 12 mm-long basalt fiber-RC beams 2T12BB2 and 2T12GB2.

In addition, it is observed that the normal steel-reinforced concrete beam has a lower number of cracks and smaller crack depth, in both the service and ultimate stages, than the BFRP and GFRP reinforced concrete beams (see Figure 16 and Figure 17). On the other hand, the use of BFRP bars leads to smaller crack depth and less cracks at the ultimate stage than the use of GFRP bars. The propagation of the cracks in the tested beams follows the traditional flexural-crack pattern. Cracks start at the pure flexure region in the tension face then propagate gradually towards the compression face where the concrete crushing occurs. The crack spacing is higher in the GFRP reinforced beam than steel and BFRP-RC beams as shown in Table 15. In general, the crack width for the BFRP and steel reinforced beams is the same at the service load stage. Then, the BFRP RC beam shows a larger crack width until the load of 65 KN, where the steel reinforced beam exhibits a sudden increase in crack width as shown in Figure 18(d). This can be attributed to the yielding of steel bars which makes the stress in the concrete increase and hence allows the cracks to open more. Beam 2T12GB1 shows a larger crack width than beams 2T12BB1 and 2T12SB1 at both the service and ultimate loading stages. The same observation is shown in Table 14 which shows the number of cracks developed as the load increases. A similar conclusion can be drawn for beams 2T12BB2 and 2T12GB2 with the 12 mm long basalt fibers as shown in Figure 18(d).

Figure 27 shows the failure mode of the aforementioned beams, where concrete crushing is the main mode of failure for the BFRP fiber-reinforced concrete beams and steel yielding is the main failure mode for the steel-reinforced concrete beam. The same failure mode was reported by Issa et al. [8] and Wang et al. [13], and it is also identical to the ACI code recommendations [18], [40] .

Moreover, concrete crushing is the main mode of failure for beam 2T12GB2. However, beam 2T12GB2 is less damaged than beam 2T12GB1 due to the larger fiber length.

(a)

(b)

(c)

(d)

Figure 27: Specimens' failure modes, (a)2T12BB1, (b)2T12GB1, (c)2T1GB2, (d) 2T12SB1

6.4. Analytical Predictions

In this section, the applicability of ACI 440-1R-06 and CSA recommendations are assessed by comparing it to the experimental results in terms of flexural capacity, mid-span deflection and cracking responses.

6.4.1. Flexural capacity. All the FRP-reinforced beams are designed to be over-reinforced in order to provide more ductility to their behavior and allow them to

fail by concrete crushing as recommended by the ACI 440-1R-06 code. Section 8.2 in the ACI 440-1R-06 FRP design guide provides a simplified design approach to calculate the nominal and design capacities of flexural members reinforced with FRP bars. The complete method, together with all the required equations, was discussed in the analytical predictions chapter. In this research, the nominal flexural capacities of all the tested beams are computed analytically based on the ACI 440-1R-06 recommendations and compared with those from the experimental results. Since there is no special code for the fiber reinforced concrete beams, the ACI 440 code is used with the assumption that all the tested beams are cast with plain concrete; therefore, the ultimate compression strain is taken as 0.003. Table 18 summarizes the analytical and experimental results for all tested beams.

Table 18: Analytical versus experimental flexural results

Sr #	**Beam**	**Mu_{exp}**	**Mu_{pred} (ACI440) ε_{cu}=0.003**	**Mu_{exp}/Mu_{pred}**
1	2T12BB1	28.2	28.1	1
2	2T16BB1	32.4	34.6	0.94
3	2T10BB1	23	23.5	0.98
4	3T10BB1	30	28	1.07
5	3T8BB1	22.2	23.8	0.93
6	2T12BS	30	26	1.15
7	2T12BP	25.2	27	0.93
8	2T12GB1	32	29	1.1
9	2T12GB2	28.2	29.2	0.97
10	2T12SB1	24.6	24.5	1
11	2T12BB2	26.4	28.3	0.93
12	2T16BB2	41.4	34.9	1.18

The table shows an acceptable difference between the experimental and predicted results using the ACI440 equations. Some of the beams showed an experimental capacity that is less than the predicted ones, which may be attributed to the accuracy and circumstances of the test.

6.4.2. Moment VS mid-span deflection. The moment versus mid-span deflection responses are plotted for both the analytical and experimental results. It can be seen from Figure 28 that the ACI 440-1R-06 code underestimates the deflection values for all the tested specimens. This can be attributed to the ductility that the section gains due to the addition of the fibers to the concrete mix. On the other hand, the steel-reinforced concrete beam shows almost the same stiffness experimentally and analytically and is much stiffer than the FRP reinforced concrete beams as shown in Figure 28(d).

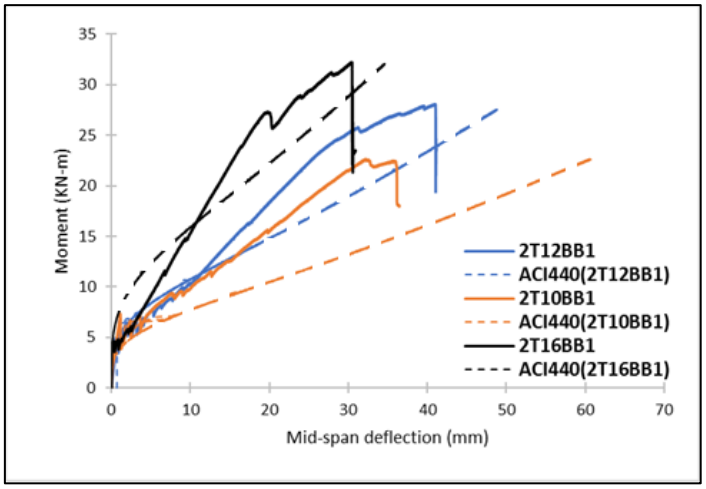

(a)

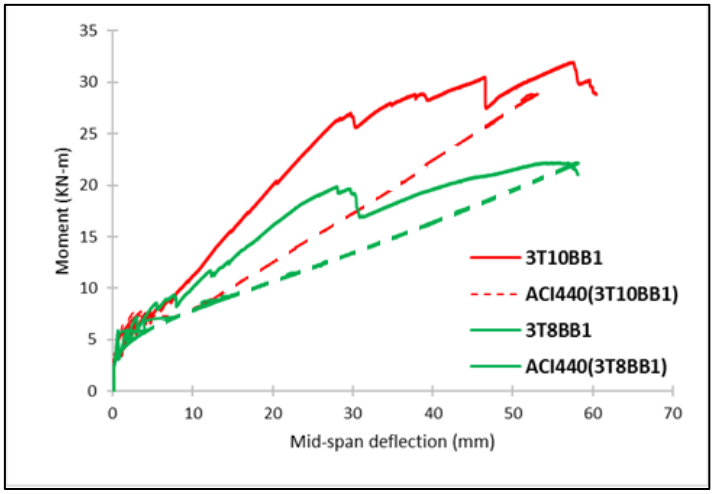

(b)

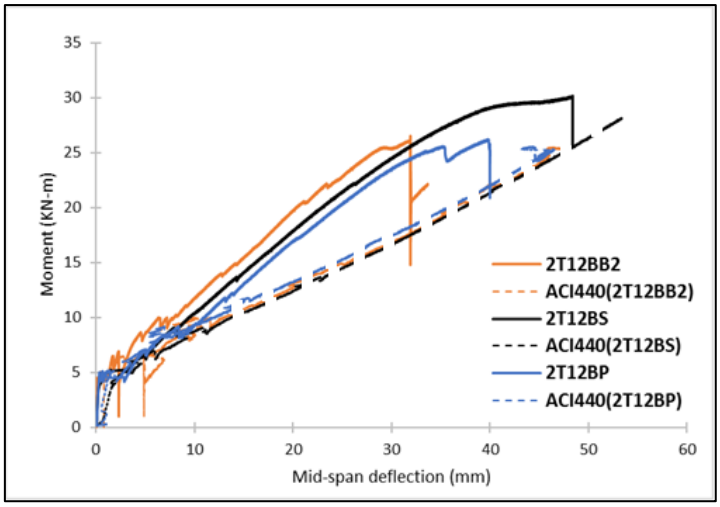

(c)

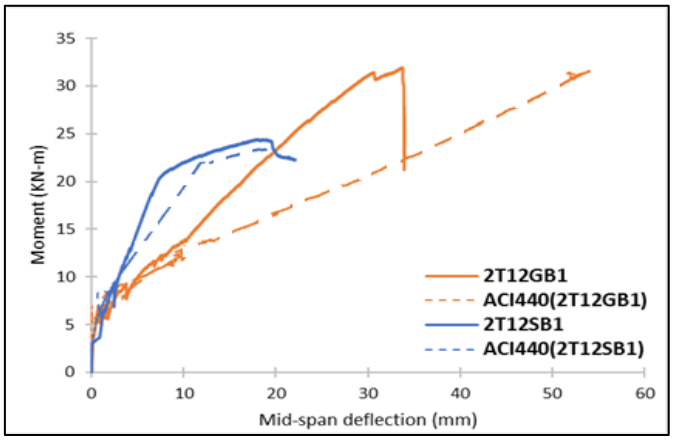

(d)

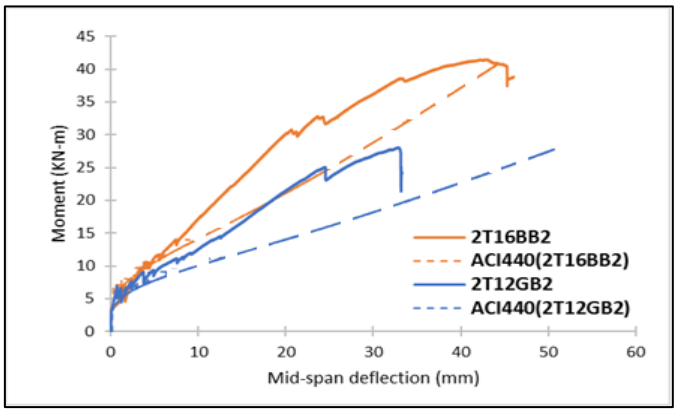

(e)

Figure 28 Analytical and experimental load vs mid-span deflection, (a) different reinforcement ratio, (b) different reinforcement ratio (3 bars); (c) different fibers; (d) different reinforcement material; (e) 12 mm basalt fibers

6.4.3. Cracking behavior. Crack spacing and crack width responses are obtained based on ACI 440-1R-06 and the Canadian guide, CSA, and are compared with the experimental results. It can be noticed from Table 16 that, generally, both codes overestimate the values of the crack width at the service stage. The effect of the fibers may be considered the main reason for this difference, since there is no guide in the literature that takes into account the effect of adding fibers to the concrete. The same observation can be seen in Table 15 for the crack spacing estimation using both ACI 440-1R-06 and CEB-FIB codes. Therefore, the addition of fibers to the concrete shows a significant effect on the cracking behavior of all tested beams. The same conclusion is reported by many researchers [8], [13], [15]

Chapter 7. Finite Element Model

In order to understand the flexural behavior of FRC beams reinforced with different types of FRP bars, it is very crucial to be able to predict and simulate their failure mechanisms. In this chapter a finite element model (FEM) was developed to investigate the flexural behavior of BFRP-FRC beams. Several research have been conducted on finite element modeling of the flexure and shear behaviors of FRP and steel-Reinforced plain concrete beams[33], [46]–[54]. This study, however, attempts to develop a nonlinear FE model that has the ability of capturing the complex behavior of fibrous concrete (FRC) beams reinforced with FRP bars in terms of moment capacity, load vs mid-span deflection, cracking behavior and failure mode.

The finite element software ABAQUS was utilized to perform a non-linear 3D analysis of the five tested beams considered in the experimental program. Four main material definitions were used in the FE modeling; the BFRP, GFRP, steel and concrete. Materials nonlinearity were considered in the FE analysis by introducing the actual elastic–plastic stress–strain relationship for the concrete. Also, the (NLGEOM) option was considered in the analysis in order to account for large deformations. The moment capacities, failure modes and moment-deflection curves were extracted from the FE model for all beams considered. These results were also verified with the experimental results. A number of 5 beams were chosen from the experimental program to be simulated using ABAQUS as shown in Table 19.

Table 19: beams for FEM

Specimen Label	Reinforcement	microfibers	f_c' (Mpa)
2T12BB1	BFRP	Basalt	45
2T10BB1	BFRP	Basalt	45
2T16BB1	BFRP	Basalt	45
2T12GB1	GFRP	Basalt	45
2T12SB1	STEEL	Basalt	45

7.1. Model Geometry

The FRC beams were modeled using a 3D solid brick element (C3D8R) with 3 degrees of freedom per node, whereas, the reinforcement including stirrups were modeled using truss elements, which only carries axial load during bending. Figure 29 shows the parts assembly of the BFRP-FRC beams as modeled in ABAQUS. The

interaction between the concrete and the reinforcement was assured to be perfectly bonded by embedding the truss elements (rebar and stirrups) inside the concrete beam as the host. Rigid steel plates were assembled at the two loading points and two supports. Normal and tangential surface-to-surface contact was defined between the rigid plate and the concrete beam using the penalty approach. Boundary conditions in terms of joints translations and displacement loadings were assigned to the rigid plates through their reference points. The same size of mesh was used for all of the assembled parts.

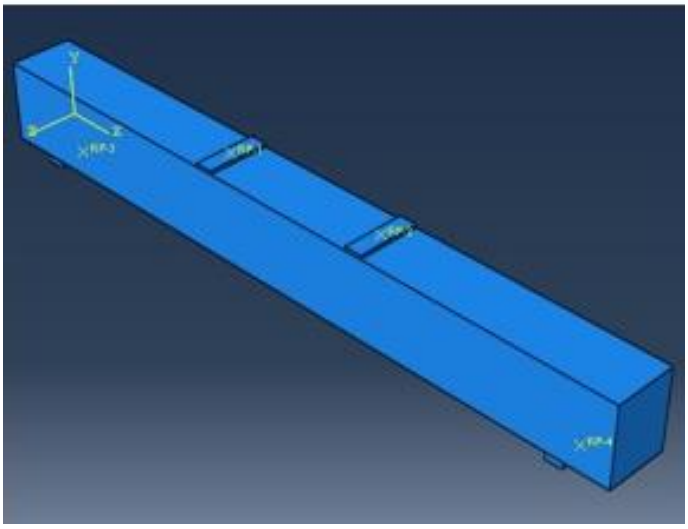

(a)

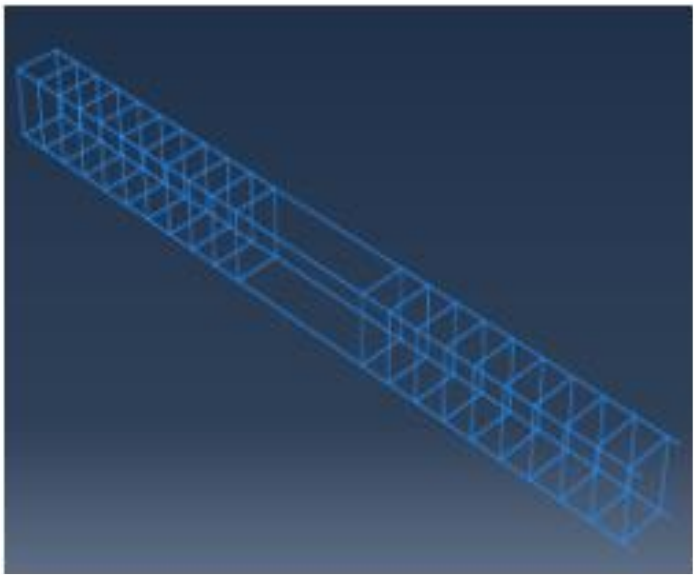

(b)

Figure 29: FEM; (a) Beam model, (b) Reinforcement model

7.2. Material Properties

The FE model utilized the experimental tests conducted for FRC concrete, BFRP, GFRP and steel in defining their properties in the numerical simulations. For concrete, the inelastic behavior was modelled using concrete damage plasticity (CDP) model based on the stress-inelastic stain data. The CDP approach permits the concept of strain hardening in compression. The uniaxial stress-strain curves for concrete in compression is shown in Figure 30. For reinforcement, the modulus of elasticity and the poisson ratio were used to define the elastic effect. The plastic effect was defined using the yield strength for the steel reinforcement and the ultimate strength for the BFRP and GFRP bars.

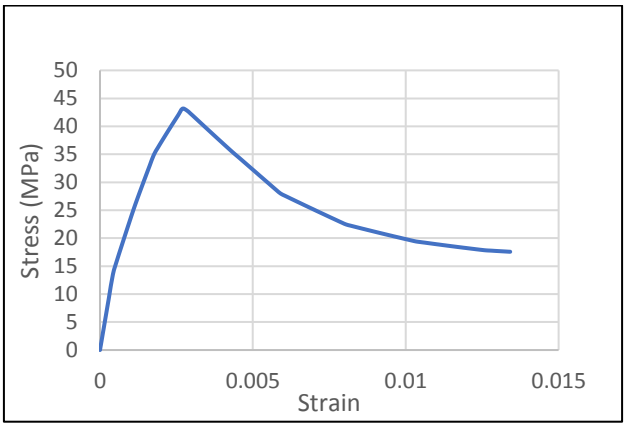

Figure 30: Stress-strain curve for a concrete cube specimen

7.3. FEM Results and Discussions

The FEM results were validated with their experimental counterparts by comparing the failure modes, cracking behavior and the moment vs mid span deflection curves for each beam. The FEM results showed a very good agreement with the results obtained from the experimental program. In addition, the failure mode for the finite element model was very close to the experimental program for all beams which is concrete crushing. The cracking behavior of the BFRP beams was pure flexural and followed the trend of the experimental outcomes as shown in Figure 31 (a and b). All cracks were pure flexural cracks developed in the tension zone and propagated towards the compression zone in the pure bending region.

The deformation capacity for the FE model was close to the experimental with an average value of 35 mm.

(a)

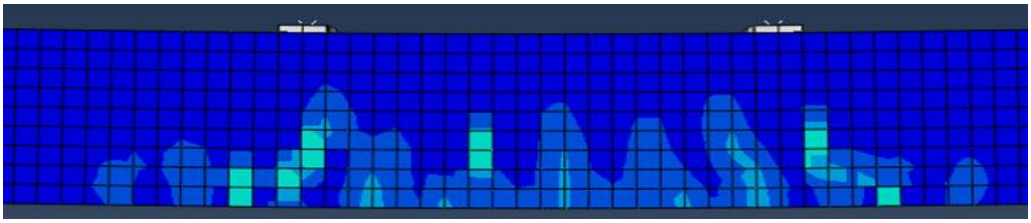

(b)

Figure 31: Crack pattern; (a) Experimental, (b) FEM

Two parameters were investigated in this study, which are the reinforcement ratio and the type of reinforcing bars. The effect of reinforcement ratio was captured by plotting load vs mid-span deflection response predicated by the FEM and compared to the experimental one for 2T10BB1, 2T12BB1 and 2T16BB1 beams as shown in Figure 32 (a-c). In general, the FEM results showed good comparisons in terms of the stiffness and load capacity. However, slight deviations were noticed in the cracking moment (load) between the FEM and experimental results for the three specimens. The moment capacity increased by increasing the reinforcement ratio as shown in Figure 32. Concrete crushing was the failure mode for all of BFRP beams. All the beams almost have the same stiffness except 2T16BB1, which has a considerably higher stiffness. In general, the addition of fibers improves the ductility of the BFRP beams and reduces the mid-span deflection.

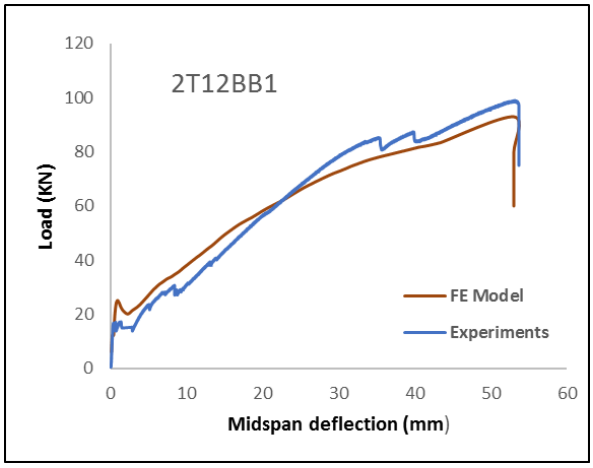

(a)

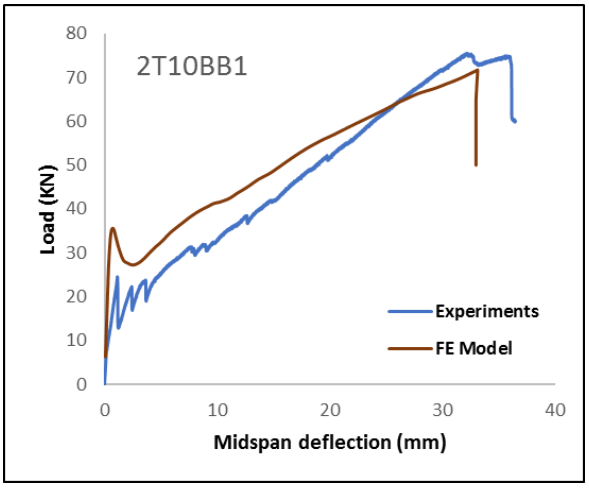

(b)

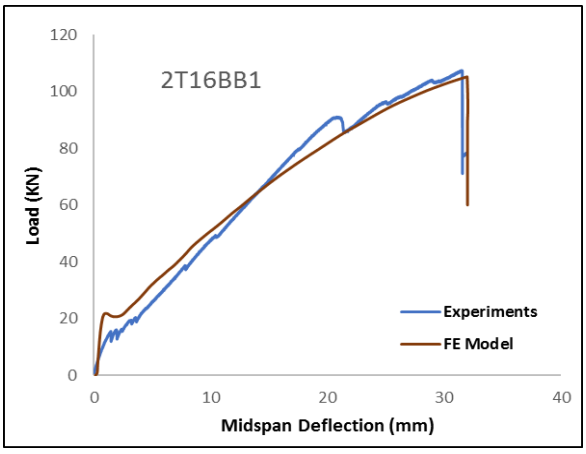

(c)

Figure 32: Load VS midspan deflection for different reinforcement ratio; (a) ρ=0.0073, (b) ρ=0.0051, (c) ρ=0.0129

Moreover, the effect of the material type of the reinforcing bars was examined through the moment vs mid-span deflection curves. Three different types of reinforcement bars of 12mm diameter were used. The corresponding load vs displacement responses are illustrated in Figure 33(b) for steel rebar, Figure 33(a) for GFRP rebar and Figure 32(a), for BFRP bars. Both BFRP- and GFRP-FRC beams have less stiffness than steel FRC beam with no clear yielding point as expected. The moment capacity for the GFRP beam was higher than BFRP and steel FRC beams.

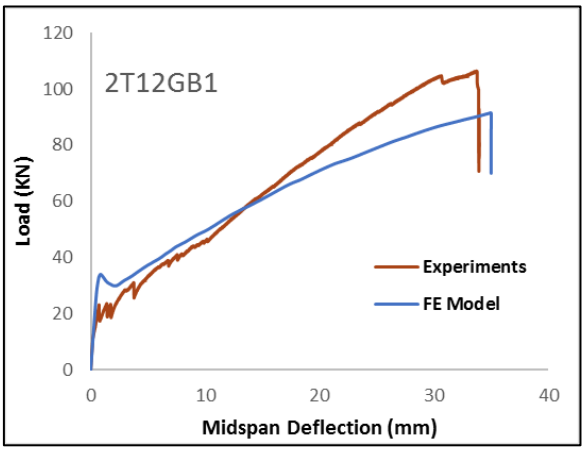

(a)

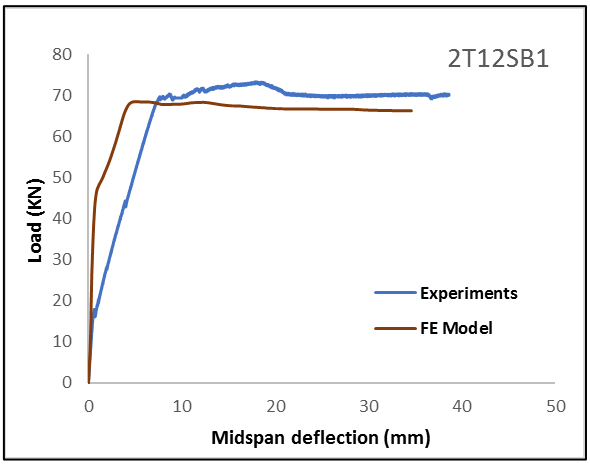

(b)

Figure 33: Load VS midspan deflection for different bar type; (a) Glass FRP, (b) steel

Chapter 8. Conclusion

This research study contains an experimental program that was conducted to investigate the effects of varying flexural reinforcement ratios using different types of reinforcement bars in concrete with basalt and synthetic fibers on the flexural behavior of BFRP-bar reinforced concrete members. Moreover, some analytical predictions are carried out to evaluate the current design codes and recommendations associated with the use of BFRP bars as flexural longitudinal reinforcement in reinforced concrete beams cast with plain and fiber-reinforced concrete. Based on the results obtained both experimentally and analytically, several conclusions and observations are drawn and listed below:

1. Increasing the BFRP reinforcement ratio results in improving the flexural capacity of BFRP beams, regardless of the concrete type. The increase was not proportional and followed the same increasing trend of ACI 440-1R-06 code equation for predicting the flexural capacity. Furthermore, increasing the reinforcement ratio has a significant contribution to the ductility and cracking behavior at different loading stages.

2. Introducing basalt and synthetic fibers to concrete increases the maximum moment capacity in FRC beams of a constant reinforcement ratio. The basalt FRC beam shows a percentage increase of 12% as compared to 19% increase when using the synthetic fiber. In addition, FRC beams fail in a less destructive manner than plain concrete beams. This is due to the ability of fibers to bridge between cracks.

3. The flexural behavior of BFRP-FRC beams improved in terms of moment capacity and curvature ductility. The section capacity was enhanced due to the increase in the ultimate concrete compression strain, which results in a larger strength contribution of BFRP bars.

4. The cracking behavior of FRC beams in terms of spacing and numbers are improved at the service and ultimate loading stages compared to plain concrete beam. The effect of basalt fibers in controlling the number of cracks is slightly better than that of synthetic fibers particularly at the service loading stage. The effect of fibers in controlling crack width at the service load stage,

corresponding to a flexural capacity of 0.3 Mu, is found to be within ACI440-1R-06 crack width limit for all of the specimens.

5. The beam with the normal steel reinforcement, shows a much higher stiffness than FRP beams which may be attributed to the lower elastic modulus of FRP material. The normal steel reinforced concrete beam has the least number of cracks and the smallest crack depth in both the service and ultimate stages, compared to the BFRP and GFRP reinforced concrete beams. Moreover, the use of FRP reinforcement reduces the curvature ductility of the beam.

6. The beams with 24 mm basalt fibers increased the flexural capacity by 12% compared to the beams with 12 mm basalt fibers. Although concrete crushing is the main mode of failure for all specimens of both basalt-fiber lengths, beams with 12 mm fiber length showed a less damaged concrete compression zone than 24 mm fiber length beams.

7. For the same reinforcement ratio, increasing the number of BFRP reinforcement bars results in approximately similar response in terms of section capacity and stiffness. However, cracking behavior and curvature ductility were improved.

8. The experimental results showed a good agreement with the analytical ones obtained using ACI equations in terms of flexural capacity, crack spacing, crack widths and mid-span deflection.

9. A nonlinear 3D finite element model was developed using ABAQUS and was validated using the results obtained from the experimental tests. The comparisons showed a very good agreement between the FEM results and the experimental ones in terms of the load (moment) capacity, the cracking behavior and the failure mode for all tested specimens. Results showed that the flexural capacity of BFRP-FRC beams considerably increases by increasing the reinforcement ratio.

10. For future studies, our model can be advanced by modeling the microfibers that introduced to the concrete, which will result in more accurate results. Therefore, the model can be used to conduct a further parametric study on the

flexural behavior of BFRP beams considering all the parameters that can affect their flexural behavior.

References

[1] L. C. Bank. *Composites for Construction*. Hoboken, New Jersey: John Wiley & Sons, 2006, pp. 67-551.

[2] J. Du, C. Wang, M. Qiao, X. Chang, and H. Chen. "Flexural behavior of concrete beams reinforced by CFRP bars," in *Int. Conf. Mech. Autom. Control Eng.*, 2010, vol. 13, no. 5, pp. 1060–1063.

[3] A. El Refai and F. Abed. "Concrete contribution to shear strength of beams reinforced with basalt fiber-reinforced bars," *J. Compos. Constr.*, vol. 20, no. 4, pp. 150-179, Dec. 2015.

[4] F. Elgabbas, E. A. Ahmed, and B. Benmokrane. "Flexural behavior of concrete beams reinforced with ribbed basalt-FRP bars under static loads," *J. Compos. Constr.*,vol 21, no. 3, pp. 195-230, Sep. 2016.

[5] F. Abed, H. El-Chabib, and M. AlHamaydeh. "Shear characteristics of GFRP-reinforced concrete deep beams without web reinforcement," *J. Reinf. Plast. Compos.*, vol. 31, no. 16, pp. 1063–1073, Aug. 2012.

[6] S. Alsayed and A. Alhozaimy. "Ductility of concrete beams reinforced with FRP bars and steel fibers," *J. Compos. Mater.*, vol. 33, no. 19, pp. 1792–1804, Oct. 1999.

[7] M. N. Habeeb and A. F. Ashour. "Flexural behavior of continuous GFRP reinforced concrete beams," *J. Compos. Constr.*, vol. 12, no. 2, pp. 115–124, Apr. 2008.

[8] M. S. Issa, I. M. Metwally, and S. M. Elzeiny. "Influence of fibers on flexural behavior and ductility of concrete beams reinforced with GFRP rebars," *Eng. Struct.*, vol. 33, no. 5, pp. 1754–1763, May. 2011.

[9] H. M. Mohamed and R. Masmoudi. "Flexural strength and behavior of steel and FRP-reinforced concrete-filled FRP tube beams," *Eng. Struct.*, vol. 32, no. 11, pp. 3789–3800, Nov. 2010.

[10] A. El Refai, F. Abed, and A. Altalmas. "Bond durability of basalt fiber – reinforced polymer bars embedded in concrete under direct pullout conditions," *J. Compos. Constr.*, vol. 19, no. 5, pp. 1–11, Dec. 2014.

[11] M. Robert and B. Benmokrane. "Behaviour of GFRP reinforcing bars subjected to extreme temperatures," *J. Compos. Constr.*, vol. 14, no.4, pp. 353–360, Nov. 2009.

[12] D. Tomlinson and A. Fam. "Performance of concrete beams reinforced with basalt FRP for flexure and shear," *J. Compos. Constr*, vol. 19, no. 2, pp. 140-150, Jun. 2014.

[13] H. Wang and A. Belarbi. "Ductility characteristics of fiber-reinforced-concrete beams reinforced with FRP rebars," *Constr. Build. Mater.*, vol. 25, no. 5, pp. 2391–2401, May. 2011.

[14] G. Wu, Z. Dong, X. Wang, Y. Zhu, and Z. Wu. "Prediction of long-term

performance and durability of BFRP bars under the combined effect of sustained load and corrosive solutions," *J. Compos. Constr.*, vol. 19, no. 3, pp. 4-15, Aug. 2014.

[15] J. M. Yang, K. H. Min, H. O. Shin, and Y. S. Yoon. "Effect of steel and synthetic fibers on flexural behavior of high-strength concrete beams reinforced with FRP bars," *Compos. Part B Eng.*, vol. 43, no. 3, pp. 1077–1086, Apr. 2012.

[16] C. E. Bakis *et al.* "Fiber-reinforced polymer composites for construction -state-of-the-art review," *J. Compos. Constr.*, vol. 6, no. May, pp. 73–87, May. 2002.

[17] L. C. Bank, T. I. Campbell, and C. W. Dolan. "Guide for the design and construction of concrete reinforced with FRP bars," U.S. ACI 440-1R, Jun. 4, 2006.

[18] T. I. Campbell, and C. W. Dolan. "Specification for carbon and glass fiber-reinforced polymer bar materials for concrete reinforcement," U.S. ACI 440, Jan. 4, 2008.

[19] G. Campione. "Simplified flexural response of steel fiber-reinforced concrete beams," *J. Mater. Civil Eng*., vol. 20, no. 4, pp. 283–293, Apr. 2008.

[20] C. High, H. M. Seliem, A. El-safty, and S. H. Rizkalla. "Use of basalt fibers for concrete structures," *Constr. Build. Mater.*, vol. 96, no.1, pp. 37–46, Oct. 2015.

[21] P. Iyer, S. Y. Kenno, and S. Das. "Mechanical properties of fiber-reinforced concrete made with basalt filament fibers," *J. Mater. Civil Eng*., vol. 27, no. 11, pp. 1–8, Nov. 2015.

[22] T. Ayub, S. M. Asce, N. Shafiq, and S. U. Khan. "Compressive stress-strain behavior of HSFRC reinforced with basalt fibers," *J. Mater. Civil Eng.*, vol. 28, no. 4, pp. 1–11, Apr. 2016.

[23] C. Jiang, K. Fan, F. Wu, and D. Chen. "Experimental study on the mechanical properties and microstructure of chopped basalt fibre reinforced concrete," *J. Mater.*, vol. 58, pp. 187–193, Jun. 2014.

[24] S. Deb and B. Tech. "The impact of Basaltic fiber on selected physical and mechanical properties of cement mortar," *Compos. Mater.*, vol. 1, no. 2, pp. 286–289.July. 2012.

[25] B. Columbia, M. East, and M. Vesuviu. *Advanced Concrete for Use in Civil Engineering.*, Cambridge: Woodhead, 2006, pp. 120-376.

[26] J. Branston, S. Das, S. Y. Kenno, and C. Taylor. "Mechanical behaviour of basalt fibre reinforced concrete," *Constr. Build. Mater.*, vol. 124, no. 1, pp. 878–886, Oct. 2016.

[27] T. Uomoto, H. Mutsuyoshi, F. Katsuki, and S. Misra. "Use of fiber reinforced polymer composites as reinforcing material for concrete.," *J. Mater. Civ. Eng.*, vol. 14, no. 3, pp. 182-191, Jun. 2002.

[28] M. A. Aiello and L. Ombres. "Structural performances of concrete beams with hybrid (fiber-reinforced polymer-steel) reinforcements," *J. Compos. Constr.*, vol. 6, no. 2, pp. 133–140, May. 2002.

[29] A. Al-tamimi, F. H. Abed, and A. Al-rahmani. “Effects of harsh environmental exposures on the bond capacity between concrete and GFRP reinforcing bars,” *Adv. Concrete Const.*, vol. 2, no. 1, pp. 1–11, Mar. 2014.

[30] A. Altalmas, A. El Refai, and F. Abed. “Bond degradation of basalt fiber-reinforced polymer (BFRP) bars exposed to accelerated aging conditions,” *Constr. Build. Mater.*, vol. 81, no. 1, pp. 162–171, Apr. 2015.

[31] A. El Refai, M.-A. Ammar, and R. Masmoudi. “Bond performance of basalt fiber-reinforced polymer bars to concrete,” *J. Compos. Constr.*, vol. 19, no. 3, p. 150-166, Jun. 2015.

[32] W. Xue, F. Peng, and Q. Zheng. “Design equations for flexural capacity of concrete beams reinforced with glass fiber – reinforced polymer bars,” *J. Compos. Const.*, vol. 20, no. 3, pp. 1–11, Jun. 2016.

[33] A. Sagher, F. H. Abed. “Finite element parametric study of the shear behavior of GFRP-RC short beams,” in *7th Int. Conf. Model. Simul. Appl. Optim (ICMSAO)*, 2017, pp. 1–5.

[34] M. W. Goldston, A. Remennikov, and M. N. Sheikh. “Flexural behaviour of GFRP reinforced high strength and ultra high strength concrete beams,” *Constr. Build. Mater.*, vol. 131, no. 30, pp. 606–617, Jan. 2017.

[35] B. S. Mebarkia, C. Vipulanandan, and A. Member. “Compressive behavior o f glass-fiber-reinforced polymer concrete,” *J. Mater. Civil. Eng.*, vol. 4, no. 1, pp. 91–105, Feb. 1992.

[36] J. Reis. “Mechanical characterization of fiber reinforced polymer concrete,” *Mater. Res.*, vol. 8, no. 3, pp. 357–360, Jul. 2005.

[37] G. Campione. “Flexural behavior of steel fibrous reinforced concrete deep beams,” *J. Struct. Eng.*, vol. 138, no 2. February, pp. 234–246, Feb. 2012.

[38] A. El Refai, F. H. Abed, and A. Al-Rahmani. “Structural performance and serviceability of concrete beams reinforced with hybrid GFRP and steel bars,” *Constr. Build. Mater.*, vol. 96, no. 1, pp. 518–529, Oct. 2015.

[39] M. A. Rashid, M. A. Mansur, and P. Paramasivam. “Behavior of aramid fiber-reinforced polymer reinforced high strength concrete beams under bending,” *J. Compos. Constr.*, vol. 9, no. 2, pp. 117–127, Apr. 2005.

[40] P. N. Balaguru, C. E. Bakis, and T. E. Bradberry. “Building code requirements for reinforced concrete,” U.S. ACI Committee 318, Nov. 5, 2014.

[41] F. Elgabbas, P. Vincent, E. A. Ahmed, and B. Benmokrane. “Experimental testing of basalt fiber-reinforced polymer bars in concrete beams,” *Compos. Part B*, vol. 91, no. 2, pp. 205–218, Apr. 2016.

[42] C. Kassem, A. S. Farghaly, and B. Benmokrane. “Evaluation of flexural behavior and serviceability performance of concrete beams reinforced with FRP bars,” *J. Compos. Const.*, vol. 15, no. 5, pp. 682–695, Oct. 2011.

[43] A. El-nemr, E. A. Ahmed, and B. Benmokrane. “Flexural behavior and serviceability of normal and high strength concrete beams reinforced with glass fiber-reinforced polymer bars,” *ACI struct. J.*, vol. 110, no. 6, pp. 1077-1087,

Nov. 2013.

[44] M. M. Rafi, A. Nadjai, F. Ali. “Experimental testing of concrete beams reinforced with carbon FRP,” *J. Compos. Mater.*, vol. 41, no. 22, p 2657-2673, Nov. 2007.

[45] M. Theriault, B. Benmokrane. “Effects of FRP reinforcement ratio and concrete strength,” *J. Compos. Const*, vol. 2, no. 2, pp. 7–16, Feb. 1998.

[46] A. Al-Rahmani and F. H. Abed. “Numerical investigation of hybrid FRP reinforced beams,” in *5th Int. Conf. Model. Simul. Appl. Optim. ICMSAO*, 2013, pp. 1-11.

[47] Y. Chi, M. Yu, L. Huang, and L. Xu. “Finite element modeling of steel-polypropylene hybrid fiber reinforced concrete using modified concrete damaged plasticity,” *Eng. structures*, vol. 148, no. 1, pp. 23–35, Oct. 2017.

[48] F. H. Abed, A. Al-rahmani, and A. H. Al-rahmani. “Finite element simulations of the shear capacity of GFRP-reinforced concrete short beams,” in *5th Int. Conf. Model. Simul. Appl. Optim. ICMSAO*, 2013, pp. 1–5.

[49] F. S. Makarem and F. H. Abed. “Nonlinear finite element modeling of dynamic localizations in high strength steel columns under impact,” *Int. J. Impact Eng.*, vol. 52, no. 1, pp. 47–61, Feb. 2013.

[50] F. H. Abed, M Saffarini, A Abdul-Latif, and G. Z. Voyiadjis. “Flow stress and damage behavior of C45 steel over a range of temperatures and loading rates,” *ASME J. Eng. Mater. Tech.*, vol. 139, no. 2, pp. 1–8, Feb. 2017.

[51] A. Tabei, F. H. Abed, G. Z. Voyiadjis, and H. Garmestani. “Constitutive modeling of Ti-6Al-4V at a wide range of temperatures and strain rates,” *Eur. J. Mech. / A Solids*, vol. 63, no. 1, pp. 128–135, Jun. 2017.

[52] F. H. Abed, S. I. Ranganathan, and M. A. Serry. “Constitutive modeling of nitrogen-alloyed austenitic stainless steel at low and high strain rates and temperatures,” *Int. J. Mech. Mater.*, vol. 77, no. 2, pp. 142–157, Oct. 2014.

[53] F. H. Abed,. F. Makarem, and G. Z. Voyiadjis. “Dynamic localizations in HSLA-65 and DH-36 structural steel at elevated temperatures,” *ASME J. Eng. Mater. Tech*, vol. 135, no. 2, pp. 1–11, Mar. 2013.

[54] F. H. Abed and F. Makarem. “Comparisons of constitutive models for steel over a wide range of temperatures and strain rates,” *ASME J. Eng. Mater. Tech*, vol. 134, no. 2, pp. 1–10, Mar. 2012.

Vita

Abdul Rahman AlHafiz was born in 1993, in Hama, Syrian Arab Republic. He received his high school certificate from Dubai National Charity School, class of 2010. He was awarded his bachelor's degree from Eastern Mediterranean University of Cyprus as of Jan 2016. Eng. Abdul Rahman received a Graduate Teaching Assistantship from AUS to work in the field planning surveying and geotechnical laboratories while completing the program requirements for the Master of Science in Civil Engineering, special concentration in Structural Engineering.